© 2016. Published by The Company of Biologists Ltd | Development (2016) 143, 2561-2572 doi:10.1242/dev.136820

RESEARCH ARTICLE

Gestational stress induces the unfolded protein response, resulting in heart defects

Hongjun Shi[1,2], Victoria C. O'Reilly[1], Julie L. M. Moreau[1], Therese R. Bewes[1], Michelle X. Yam[1], Bogdan E. Chapman[3,*], Stuart M. Grieve[3,4,5], Roland Stocker[1,6], Robert M. Graham[1,2,6], Gavin Chapman[1,2], Duncan B. Sparrow[1,2,‡] and Sally L. Dunwoodie[1,2,6,‡]

ABSTRACT

Congenital heart disease (CHD) is an enigma. It is the most common human birth defect and yet, even with the application of modern genetic and genomic technologies, only a minority of cases can be explained genetically. This is because environmental stressors also cause CHD. Here we propose a plausible non-genetic mechanism for induction of CHD by environmental stressors. We show that exposure of mouse embryos to short-term gestational hypoxia induces the most common types of heart defect. This is mediated by the rapid induction of the unfolded protein response (UPR), which profoundly reduces FGF signaling in cardiac progenitor cells of the second heart field. Thus, UPR activation during human pregnancy might be a common cause of CHD. Our findings have far-reaching consequences because the UPR is activated by a myriad of environmental or pathophysiological conditions. Ultimately, our discovery could lead to preventative strategies to reduce the incidence of human CHD.

KEY WORDS: FGF signaling, Heart development, Hypoxia, Unfolded protein response

INTRODUCTION

Congenital heart disease (CHD) is an abnormality in the structure or function of the heart that arises before birth. It is the most common form of human birth defect, with an incidence of ∼9 per 1000 live births (van der Linde et al., 2011). The etiology of CHD is complex, with both genetic and environmental factors playing a role. Genetic factors have been widely investigated (reviewed by Andersen et al., 2014; Fahed et al., 2013). However, only ∼20% of CHD cases can be attributed to a specific genetic cause (Blue et al., 2012). Thus, non-genetic factors are likely to be important in human heart development. This idea is supported by the large phenotypic variability seen between individuals with the same genetic mutation (Schott et al., 1998; Benson et al., 1999), and this is also true with variable heart defects in inbred mice (Abu-Issa et al., 2002). Epidemiological studies have identified significant environmental risk factors for human CHD, including maternal exposures to alcohol, isotretinoin, thalidomide, antiseizure medications, antiretroviral medications, environmental teratogens and infectious agents. Embryo hypoxia is another well-recognized risk factor caused by smoking, living at high altitude, maternal diabetes, high body mass index, hypertension or prescription medications (Watkins et al., 2003; Jenkins et al., 2007; Zheng et al., 2013; Webster et al., 2014; Ornoy et al., 2015; Ramakrishnan et al., 2015; Sullivan et al., 2015). The specific effects of environment on embryonic development have been studied by exposing pregnant animals to a variety of conditions. Hypoxia has been studied in this way for almost 200 years, causing a variety of birth defects, including heart defects (Geoffroy Saint Hilaire, 1820; Ingalls et al., 1952; Sparrow et al., 2012). We have recently shown that short-term gestational hypoxia significantly increases the penetrance and severity of vertebral defects in mouse models of congenital scoliosis (Sparrow et al., 2012). At the molecular level, hypoxia disrupts embryonic FGF signaling, leading to a temporary failure of somitogenesis.

Heart formation in vertebrates has been well studied (reviewed by Miquerol and Kelly, 2013). The linear heart tube forms from the first heart field (FHF). These cells contribute mainly to the left ventricle and both atria of the mature heart. The linear heart tube elongates and loops to the right, driven by the addition of second heart field (SHF) cells to the arterial and venous poles. These cells contribute mostly to the right ventricle and inflow/outflow regions of the heart. The proliferation of SHF cells is controlled by FGF and β-catenin/WNT signaling, and their subsequent differentiation is controlled by BMP and non-canonical WNT pathways. Perturbation of proliferation, or premature activation of differentiation or apoptosis, for example by conditional deletion of FGF signaling components in the SHF, results in OFT elongation, alignment and septation defects (Hutson et al., 2006; Ilagan et al., 2006; Park et al., 2006). In humans such defects include membranous ventricular septal defects (VSDs), persistent truncus arteriosus (PTA), double outlet right ventricle (DORV), transposition of the great arteries (TGA), overriding aorta (OA) and tetralogy of Fallot (TOF), and account for as much as 30-60% of all human CHD (Thom et al., 2006; Bruneau, 2008).

Here we present evidence that short-term gestational hypoxia can perturb mammalian heart formation, resulting in defects of OFT alignment and/or elongation. We show that hypoxic exposure results in reduced cellular proliferation in the SHF and elsewhere. In the SHF this is likely to be due to a downregulation of FGF signaling, mediated by the specific loss of the receptor FGFR1. We show that hypoxia induces the unfolded protein response, causing a global downregulation of protein translation. Since FGFR1 protein has a short half-life (Haugsten et al., 2005), this results in rapidly reduced receptor and signaling levels. Our findings might provide a mechanism for the genesis of some of the 80% of cases of human

[1]The Victor Chang Cardiac Research Institute, Sydney, New South Wales 2010, Australia. [2]St Vincent's Clinical School, Faculty of Medicine, University of New South Wales, Sydney, New South Wales 2010, Australia. [3]School of Molecular Bioscience, University of Sydney, Sydney, New South Wales 2006, Australia. [4]Sydney Translational Imaging Laboratory, Sydney Medical School, University of Sydney, Sydney, New South Wales 2006, Australia. [5]Department of Radiology, Royal Prince Alfred Hospital, Sydney, New South Wales 2050, Australia. [6]School of Biotechnology and Biomolecular Sciences, Faculty of Science, University of New South Wales, Sydney, New South Wales 2052, Australia.
*Deceased

‡Authors for correspondence (s.dunwoodie@victorchang.edu.au; duncan.sparrow@dpag.ox.ac.uk)

S.L.D., 0000-0002-2069-7349

Received 4 March 2016; Accepted 20 May 2016

Development (2016) 143, 2561-2572 doi:10.1242/dev.136820

CHD that remain unexplained by a purely genetic etiology. This mechanism is also likely to apply to birth defects in addition to CHD, as FGF signaling is required for numerous processes during embryogenesis.

RESULTS

In utero exposure of mouse embryos to lowered oxygen levels perturbs cardiac outflow tract formation

We investigated if exposure of mouse embryos to hypoxia *in utero* induces heart defects. Previous studies exposing mice to hypoxia (Ingalls et al., 1952) induced a low rate of VSDs. We performed similar experiments using more extreme hypoxia to maximize the rate of induced heart defects. Mice can tolerate as low as 5.5% oxygen at normal atmospheric pressure (Sparrow et al., 2012). We therefore exposed pregnant C57BL/6J mice to 5.5% oxygen for 8 h (hypoxia), and then returned them to room air (normoxia) until embryonic day (E) 17.5, when embryonic heart morphology was examined (Table 1). Groups of pregnant mice were exposed on different days encompassing heart development (E7.5-10.5). Heart defects were observed in some embryos exposed from E8.5-10.5, with a statistically significant peak at E9.5. At this stage, 21/48 embryos had heart defects. By contrast, low oxygen exposure did not significantly increase the incidence of embryo death, except at E10.5. All abnormal embryos exposed at E9.5 (21/21) had defects typical of a disruption of outflow tract (OFT) alignment or elongation (VSD, OA, DORV, TGA), while some had additional defects (Table S1). Thus, low oxygen exposure perturbed cardiac OFT alignment development with maximum effect at E9.5.

Alteration in cardiac OFT phenotype is apparent from E10.5

To determine the developmental origin of the cardiac defects, we examined OFT morphology in embryos exposed to 5.5% oxygen at E9.5 for 8 h and then allowed to develop in normoxia for a further 16-24 h. Control and exposed embryos were matched for somite number (range 33-38), and the OFT myocardium visualized by whole-mount myosin heavy chain (MHC) immunostaining. Optical projection tomography (OPT) was used to construct three-dimensional representations of the OFT myocardium (Fig. 1A,B). The majority of exposed embryos had altered OFT morphology, with a shorter distal OFT and an altered angle between proximal and distal OFT. There was a strong positive correlation between these parameters for control embryos (Fig. 1C, black points, P=0.0086) but not for exposed embryos (Fig. 1C, red points, P=0.3221). Thus, hypoxia-induced cardiac defects may result from a perturbation of distal OFT formation.

Low oxygen exposure affects proliferation in the SHF

The OFT forms primarily from cells of two embryonic lineages: cardiac progenitors of the SHF and cardiac neural crest cells (reviewed by Kelly, 2012; Neeb et al., 2013). Disruption of SHF development can result in defective OFT elongation, alignment and/or septation. Such defects can arise from activated apoptosis (Ilagan et al., 2006), premature differentiation (Liao et al., 2008) or reduced cell proliferation (Xu et al., 2004; Ilagan et al., 2006). No apoptosis was detected by active/pro-caspase 3 or TUNEL staining in the SHF, OFT or myocardium of control or exposed embryos (Fig. 1D,E, Fig. S1A-T). However, increased numbers of apoptotic cells were present in the neuroepithelium of the posterior part of the neural tube, otic vesicle and gut of exposed embryos, confirming that we were able to detect apoptotic cells by these techniques (Fig. S1A-T). Likewise, we did not detect any change in expression levels or location of the myocyte differentiation marker MHC between control and exposed embryos (Fig. 1G,H). By contrast, there was a clear reduction in the extent of proliferation in the SHF, OFT myocardium, branchial arch and forebrain in exposed embryos (Fig. 1J-L, Fig. S1U-Z,A′-C′). Quantification of the percentage of phosphorylated histone H3-positive nuclei indicated that proliferation in the SHF and forebrain was more affected than that in the myocardium or branchial arch. Thus, low oxygen exposure results in a significant reduction of SHF cell proliferation, but does not induce apoptosis or premature differentiation.

Low oxygen exposure reduces FGF signaling in the SHF

We have shown that low oxygen exposure *in utero* reduces FGF signaling in the presomitic mesoderm (PSM) (Sparrow et al., 2012). In the SHF, reduction or loss of FGF signaling causes reduced cell proliferation and OFT defects (Hutson et al., 2006; Park et al., 2006, 2008; Zhang et al., 2008). We therefore examined the expression of direct target genes of FGF signaling in the SHF. *Spry1*, *Spry2* and *Spry4* transcripts in the SHF were significantly reduced after 8 h exposure in the SHF (Fig. 2A-C, Fig. S2N-Q). To gauge the dynamics of FGF signaling disruption, we exposed embryos for 1, 2, 4 or 8 h to 5.5% oxygen and then examined *Spry2* transcript levels. The significant reduction in transcript levels in the SHF was only observed in embryos exposed for 8 h (Fig. S2A-F).

We next examined a more upstream component of FGF signal transduction. Depending on cellular context, FGF signal transduction can occur through three pathways: MAPK (ERK), AKT and PKCγ (Dorey and Amaya, 2010). ERK is the main pathway used by cells of the SHF (Ilagan et al., 2006; Zhang et al., 2008). Phosphorylated ERK1/2 (also known as MAPK3/1) was significantly reduced in the SHF after 8 h exposure (Fig. 2D-F). To investigate the dynamics of phosphorylated ERK1/2 loss, levels were examined after 0.5, 1, 2, 4 or 8 h exposure (Fig. S2G-M). As little as 1 h exposure caused a significant loss of phosphorylated ERK1/2. Thus, the reduced proliferation in SHF cardiac progenitor cells is likely to be due to reduced FGF signaling, and this occurs extremely rapidly upon exposure to hypoxia.

Low oxygen exposure reduces FGFR1 levels in the SHF

There are many ways by which hypoxia might perturb FGF signaling. The simplest model is that receptor or ligand levels are

Table 1. *In utero* low oxygen exposure induces heart defects

	Heart morphology					
Exposure stage	Normal	Abnormal	Abnormal (%)	*P*-value	Resorbed (%)	*P*-value
Control	31	2	6.1	–	8.3	–
E7.5	27	0	0	0.30	3.8	0.32
E8.5	33	7	17.5	0.13	8.9	0.62
E9.5	27	21	43.8	0.0001	11.9	0.42
E10.5	29	7	19.4	0.10	33.9	0.004

P-values were obtained by one-tailed Fisher's exact test.

Development (2016) 143, 2561-2572 doi:10.1242/dev.136820

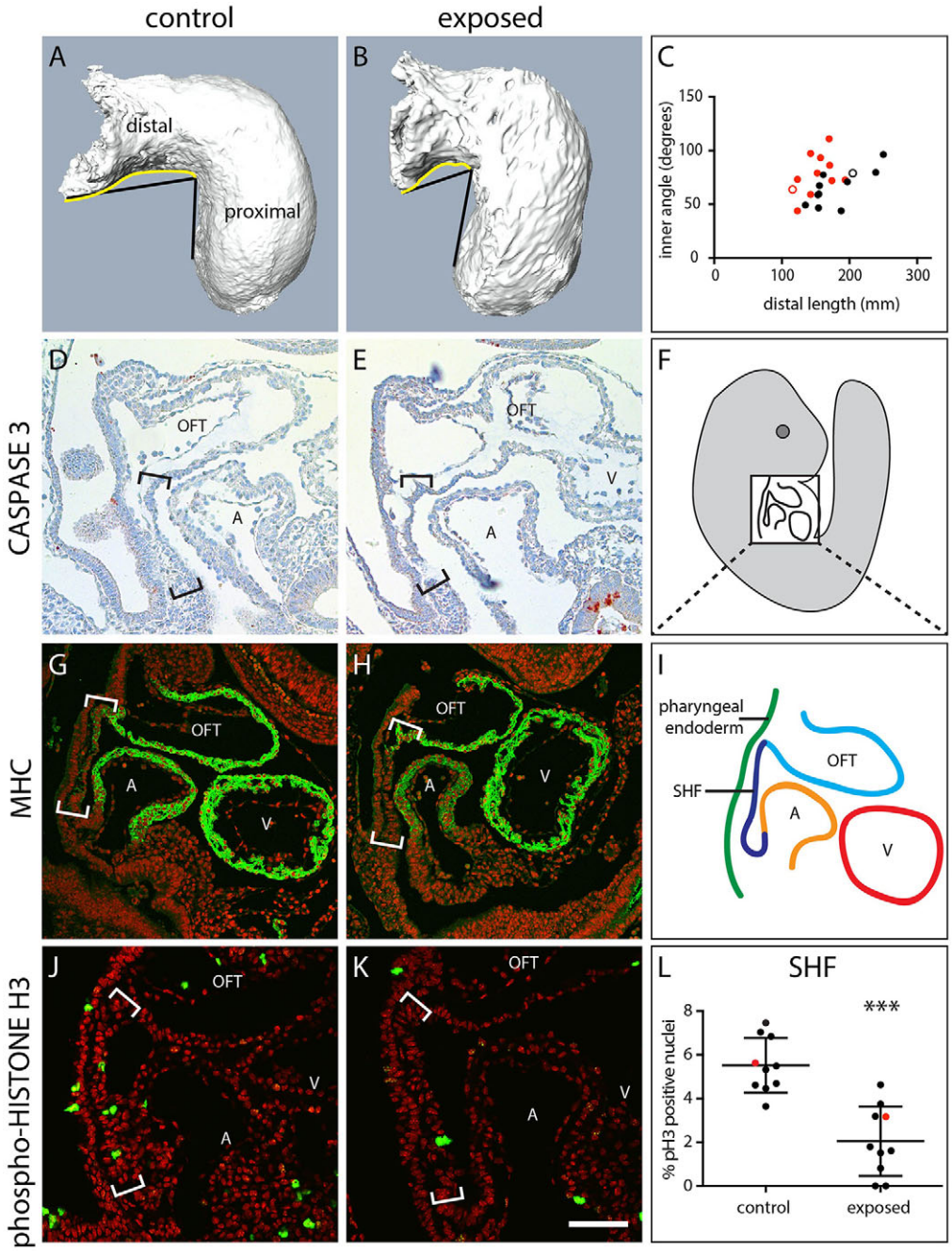

Fig. 1. Effects of low oxygen exposure of E9.5 mouse embryos on OFT morphology and on apoptosis, differentiation and proliferation of SHF cells. (A-C) Comparison of three-dimensional reconstructions of control (*n*=11) and hypoxia-exposed (8 h, *n*=11) E10.5 OFT generated by optical projection tomography (OPT). Representative images are shown of OFT from control (A) and exposed (B) embryos. Yellow lines indicate the measured distal OFT length, and black lines indicate the angle measured between the distal and proximal OFT. (C) The relationship between distal OFT length and angle between distal and proximal OFT at E10.5 for control (black dots) and exposed (red dots) embryos. The measurements for the images shown in A and B are indicated by open circles in black and red, respectively. Spearman correlation *P*-values were 0.0086 (control) and 0.3221 (exposed). (D-L) Comparison of protein levels in control and exposed E9.5 mouse embryos using immunohistochemistry on sagittal paraffin sections. (D,E) Comparison of active/pro-caspase 3 levels (*n*=10 control and *n*=10 exposed, red), (G,H) myosin heavy chain (MHC, *n*=10 control and *n*=19 exposed, green) and (J,K) phospho-histone H3 (*n*=10 control and *n*=10 exposed, green). Sections were counterstained with Hematoxylin (D,E, light blue) or TO-PRO-3 (G,H,J,K, red). For clarity, in J,K the brightness levels in the green channel only were increased. (F,I) Diagrams indicating the relative positions of the SHF (dark blue), pharyngeal endoderm (green), OFT (light blue) and left ventricle (V, red) and left atrium (A, orange) in a sagittal section of an E9.5 embryo. (L) Quantification of percentage phospho-histone H3-positive nuclei. Red dots indicate quantification of the images shown in J and K. ***P<0.001. For sections, rostral is to the top and caudal to the bottom. Location of the SHF is indicated by brackets. Scale bar in K: 80 µm in A,B,J,K; 130 µm in D,E; 140 µm in G,H. See also Fig. S1.

reduced directly in response to cellular hypoxia. FGF signaling in the SHF involves the ligands FGF8 (Brown et al., 2004; Ilagan et al., 2006; Park et al., 2006) and FGF10 (Marguerie et al., 2006; Watanabe et al., 2010) and the receptors FGFR1 and FGFR2 (Marguerie et al., 2006; Park et al., 2008; Zhang et al., 2008). We focused on FGF8 and FGFR1, as these are prominent in SHF formation (Marguerie et al., 2006; Park et al., 2008; Watanabe et al., 2010). Levels of *Fgf8* transcripts were significantly reduced in the

Development (2016) 143, 2561-2572 doi:10.1242/dev.136820

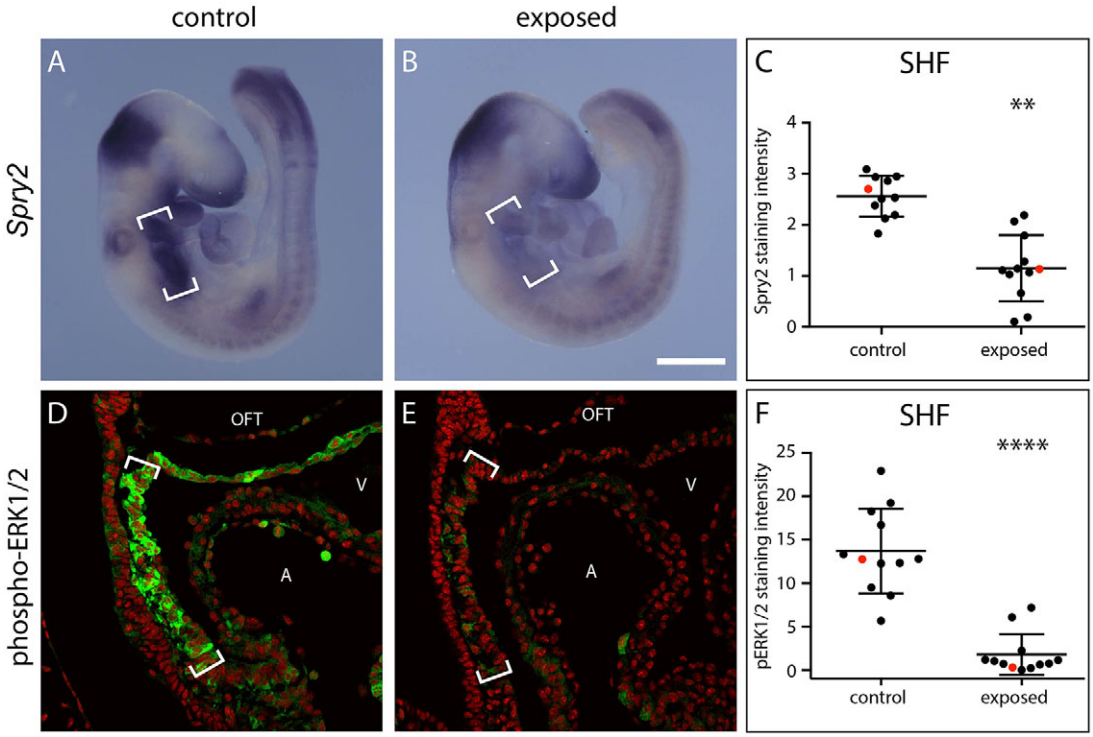

Fig. 2. Effects of low oxygen exposure of E9.5 mouse embryos on FGF signaling targets in the SHF. (A-C) Comparison of expression levels of *Spry2* in control (A, *n*=11) and hypoxia-exposed (8 h, B, *n*=12) E9.5 mouse embryos by whole-mount RNA *in situ* hybridization. (C) Quantification of levels of *Spry2* transcript in the SHF. Red dots indicate values for the embryos shown in A and B. (D-F) Comparison of phospho-ERK1/2 (green) protein levels in control (D, *n*=12) and exposed (E, *n*=12) E9.5 mouse embryos by immunohistochemistry on sagittal paraffin sections. Nuclei were stained with TO-PRO-3 (red). (F) Quantification of phospho-ERK1/2 levels in the SHF. Red dots indicate values for the embryos depicted in D and E. ***P*<0.01, ****P*<0.001. Location of the SHF is indicated by brackets. Scale bar in B: 500 µm in A,B; 80 µm in D,E. See also Fig. S2.

SHF from 4 h exposure, but not after shorter exposures (Fig. 3A-C, Fig. S3A-F). Thus, *Fgf8* transcript levels were not reduced until well after phosphorylated ERK1/2 levels were significantly reduced (4 h compared with 0.5 h). This suggests that the *Fgf8* gene might itself be a target of FGF signaling, and that its reduced transcription is a consequence, rather than the cause, of reduced FGF signaling. This is supported by the observation that conditional knockout of *Fgfr1* in the midbrain-hindbrain boundary greatly reduces FGF signaling and abolishes *Fgf8* expression (Jukkola et al., 2006).

We next examined FGFR1 protein expression. In control embryos, FGFR1 protein was concentrated in perinuclear cytoplasmic puncta, with lower levels of background staining throughout the cell (Fig. 3D). This is consistent with previous observations in different cell types *in vivo* and *in vitro* (Prudovsky et al., 1994; Ozaki et al., 2000). The puncta co-stained with the *cis*-Golgi protein GM130 (also known as GOLGA2) (Fig. 3E,F). By contrast, after 8 h exposure there was a reduction in both total FGFR1 (7/10 embryos, Fig. 3G) and Golgi-localized FGFR1 (8/10 embryos, Fig. 3K). Concomitantly, Golgi subcellular localization did not appear to be affected (Fig. 3E,F,I,J). Low oxygen exposure had a rapid effect on FGFR1 protein expression, with exposure for as little as 1 h resulting in a significant loss of Golgi-localized FGFR1 protein and total FGFR1 significantly reduced after 4 h exposure (Fig. S3G-T). We confirmed this reduction by immunoblot of whole-embryo extracts (Fig. 3O, Fig. S3B′). To assess the specificity of FGFR1 loss, we examined the protein expression of another receptor tyrosine kinase expressed in the SHF, namely PDGFRβ. PDGFRβ protein was present throughout the cytoplasm and plasma membrane of SHF cells at equivalent levels in control and exposed embryos (Fig. 3L-N, Fig. S3U-A′). Thus, FGFR1 protein levels are rapidly reduced in the SHF in response to low oxygen exposure, and there is some specificity to this response.

SHF cells in embryos exposed to lowered oxygen levels *in utero* are hypoxic

We next investigated how hypoxia causes FGFR1 protein loss. Maternal low oxygen exposure is likely to have many effects on the embryo. Previously, we have shown that the embryonic myocardium is particularly susceptible to low oxygen exposure (O'Reilly et al., 2014). We therefore investigated whether the SHF was similarly affected. We measured embryonic cellular oxygen levels using the compound Hypoxyprobe (Raleigh et al., 1999). Pregnant mice were injected with Hypoxyprobe and then exposed to 5.5% oxygen for 3 h. Limited staining was detected in control embryos under these conditions (Fig. 4A,B). By contrast, there was strong staining throughout exposed embryos, including the SHF (Fig. 4C,D).

The response to cellular hypoxia in mammalian embryos is mediated by hypoxia inducible factor (HIF1) (reviewed by Dunwoodie, 2009). The HIF1α subunit of this transcription factor is rapidly degraded in normoxia (Wang et al., 1995), but it is stabilized and transported to the nucleus when cellular oxygen levels fall below 2% (Jiang et al., 1996). Nuclear HIF1α staining was detected in the myocardium of embryos after as little as 0.5 h exposure (Fig. 4E,F,H, Fig. S4A-H,M) (O'Reilly et al., 2014). Nuclear staining was also visible in the gut (Fig. S4N). No nuclear staining of HIF1α was visible in the SHF of embryos exposed to low oxygen (Fig. 4E-G), despite these cells being hypoxic, although there was a slight increase in the total amount of HIF1α staining.

Development (2016) 143, 2561-2572 doi:10.1242/dev.136820

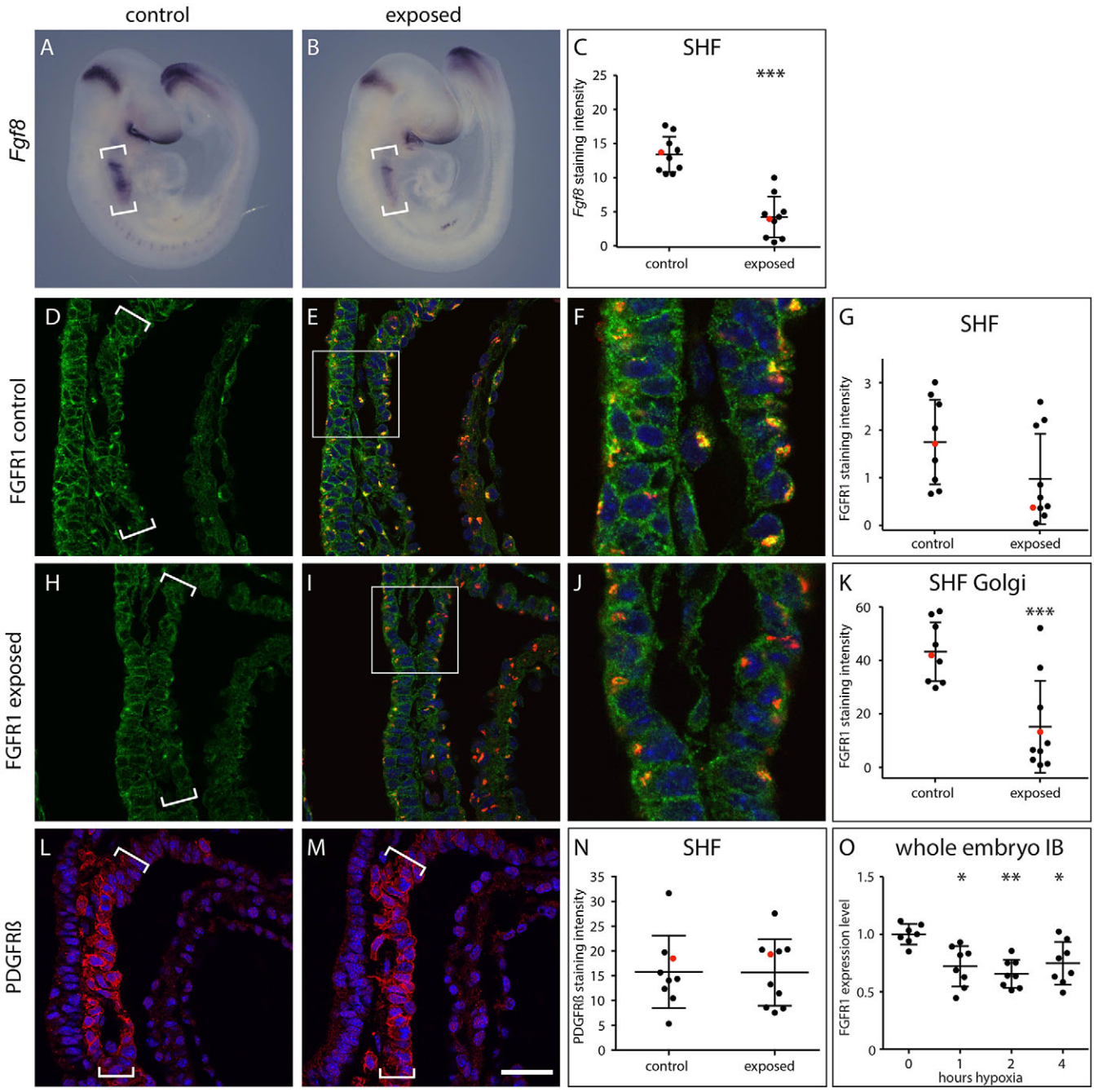

Fig. 3. Effects of low oxygen exposure of E9.5 mouse embryos on FGF signaling components in the SHF. (A-C) Comparison of expression levels of *Fgf8* in control (A, *n*=10) and hypoxia-exposed (8 h, B, *n*=10) embryos by whole-mount RNA *in situ* hybridization. (C) Quantification of *Fgf8* transcript levels in the SHF. Red dots indicate values for the embryos shown in A and B. (D-K) Comparison of FGFR1 (green) protein levels in control (D, *n*=9) and exposed (8 h, H, *n*=10) embryos by immunohistochemistry on sagittal paraffin sections. (E,I) Merged images showing FGFR1 (green), Golgi stained for GM130 (red) and nuclei stained with TO-PRO-3 (blue). (F,J) Magnified views of the boxed regions in E and I. (G) Quantification of total FGFR1 protein levels in the SHF. (K) Quantification of FGFR1 protein levels in the Golgi of the SHF. Red dots indicate values for the embryos shown in D and H. (L-N) Comparison of PDGFRβ (red) protein levels in control (L, *n*=9) and exposed (8 h, M, *n*=10) embryos by immunohistochemistry on sagittal paraffin sections. Nuclei were stained with TO-PRO-3 (blue). (N) Quantification of PDGFRβ protein levels in the SHF. Red dots indicate values for the embryos shown in L and M. (O) Quantification from immunoblots of total protein levels of FGFR1 in whole E9.5 embryos exposed to normoxia (0 h) or 5.5% oxygen for 1-4 h. **P*<0.05, ***P*<0.01, ****P*<0.001. Location of the SHF is indicated by brackets. Scale bar in M: 500 µm in A,B; 40 µm in D,E,H,I,L,M; 15 µm in F,J. See also Fig. S3.

SHF cells in embryos exposed to lowered oxygen levels *in utero* induce the unfolded protein response

One cellular consequence of hypoxia is disruption of protein folding in the endoplasmic reticulum (ER) (Feldman et al., 2005). If such disruption is severe, the unfolded protein response (UPR) will be induced. This is a coordinated cellular program that reduces the rate of protein synthesis generally, increases the expression of molecular chaperones to assist protein refolding,

Development (2016) 143, 2561-2572 doi:10.1242/dev.136820

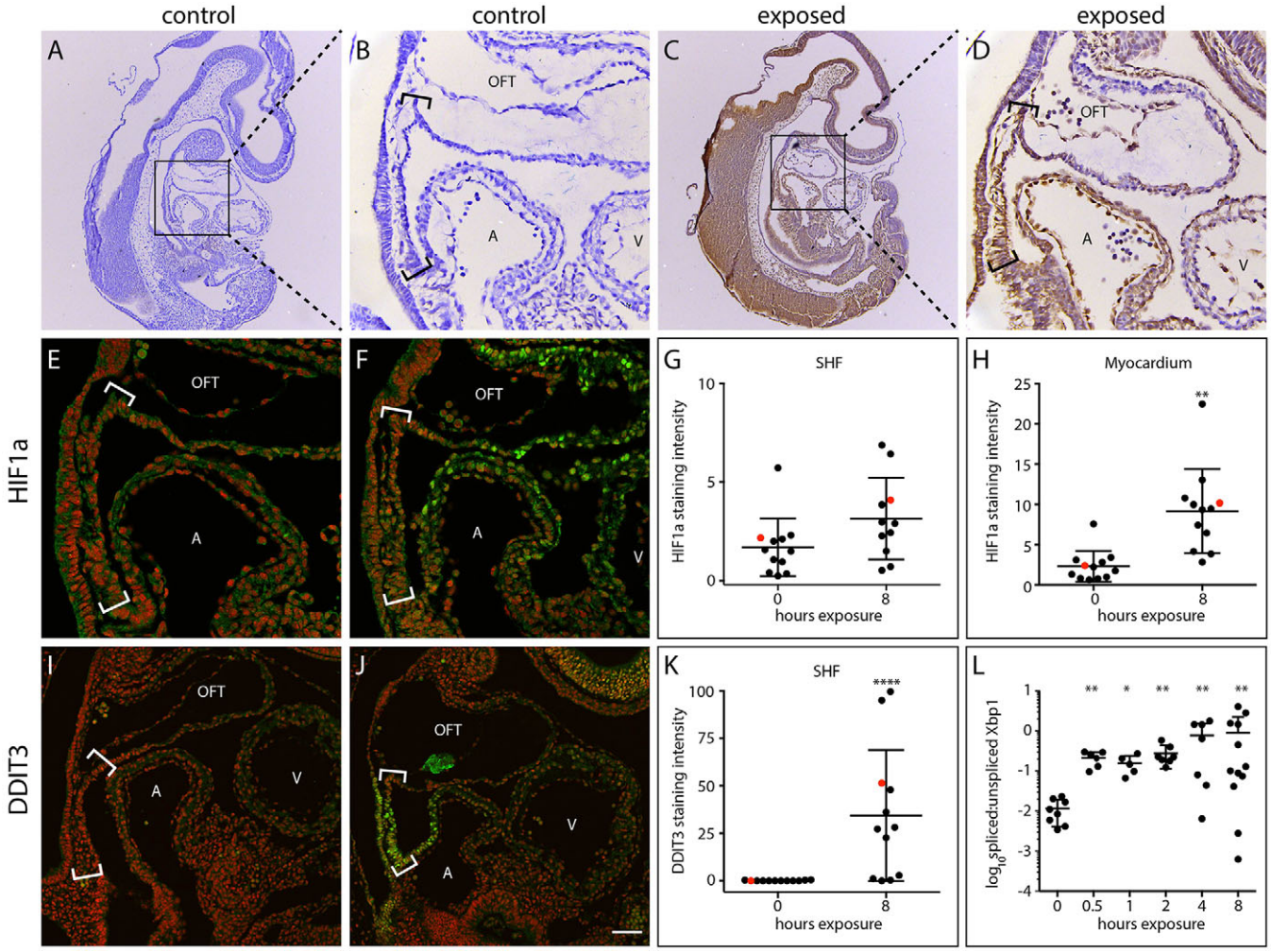

Fig. 4. SHF cells in embryos exposed to lowered oxygen levels *in utero* are hypoxic and induce the UPR. (A-D) Comparison of cellular hypoxia levels in control (A,B, *n*=8) and hypoxia-exposed (3 h, C,D, *n*=8) E9.5 mouse embryos by immunohistochemistry against Hypoxyprobe (brown) on sagittal paraffin sections. Magnified views of the boxed regions in A and C are shown in B and D. (E-H) Comparison of HIF1α (green) protein levels in control (E, *n*=12) and exposed (F, *n*=11) embryos by immunohistochemistry on sagittal paraffin sections. Nuclei were stained with TO-PRO-3 (red). (G,H) Quantification of HIF1α levels in the SHF (G) and myocardium (H). Red dots indicate values for the embryos shown in E and F. (I-K) Comparison of DDIT3 (green) protein levels in control (I, *n*=12) and exposed (8 h, J, *n*=12) embryos by immunohistochemistry on sagittal paraffin sections. Nuclei were stained with TO-PRO-3 (red). (K) Quantification of DDIT3 expression levels in the SHF. Red dots indicate values for the embryos shown in I and J. (L) Quantification of levels of spliced *Xbp1* transcripts in whole-embryo RNA extracts from control (*n*=8) and exposed embryos. Exposure times were 0.5 (*n*=6), 1 (*n*=5), 2 (*n*=7), 4 (*n*=7) and 8 (*n*=12) h. **P*<0.05, ***P*<0.01, *****P*<0.0001. Location of the SHF is indicated by brackets. Scale bar in J: 80 µm in A,C,E,F; 20 µm in B,D; 140 µm in I,J. See also Fig. S4.

upregulates the ER-associated degradation (ERAD) pathway to degrade terminally misfolded proteins, and induces apoptosis if ER stress persists (Kitamura, 2013).

We examined the expression of a late marker of the UPR, DNA damage-inducible transcript 3 (DDIT3, also known as CHOP) to determine if the UPR is induced in low oxygen-exposed embryos. DDIT3 was robustly induced in the SHF of 8/12 embryos after 8 h exposure, and in a subset of exposed embryos from as early as 2 h (Fig. 4I-K, Fig. S4O-U). We also analyzed the production of an immediate early marker of the UPR, namely spliced *Xbp1* transcript. Significant levels of spliced *Xbp1* were detectable by qPCR in whole-embryo RNA extracts after as little as 0.5 h exposure (Fig. 4L). This suggests that the UPR is rapidly induced in embryos exposed to low oxygen levels. Thus, the specific loss of FGFR1 protein expression in embryos exposed to low oxygen levels correlates with both hypoxia and induction of the UPR in the SHF.

FGFR1 protein levels are reduced *in vitro* in response to hypoxia and other cellular stressors

We next developed an *in vitro* model system to investigate the molecular mechanism by which FGFR1 is lost in response to hypoxia. We used mouse muscle satellite C2C12 cells because they express FGFR1 and can activate the FGF pathway through ERK (Erck et al., 1998). Cells were cultured for 1-4 h in 0.1% oxygen and then protein extracts analyzed by immunoblot (Fig. 5A,B). In keeping with our *in vivo* results, levels of FGFR1 and phosphorylated ERK1/2 were significantly reduced by hypoxia, whereas total ERK1/2 and β-tubulin levels remained constant. The degree of reduction was similar to that observed in immunoblots of whole embryos exposed to 5.5% oxygen for 1-4 h (Fig. 3O). Exposed cells also had significantly increased levels of the translation initiation factor phosphorylated EIF2α and DDIT3, indicating robust UPR activation (Fig. 5A,B).

Development (2016) 143, 2561-2572 doi:10.1242/dev.136820

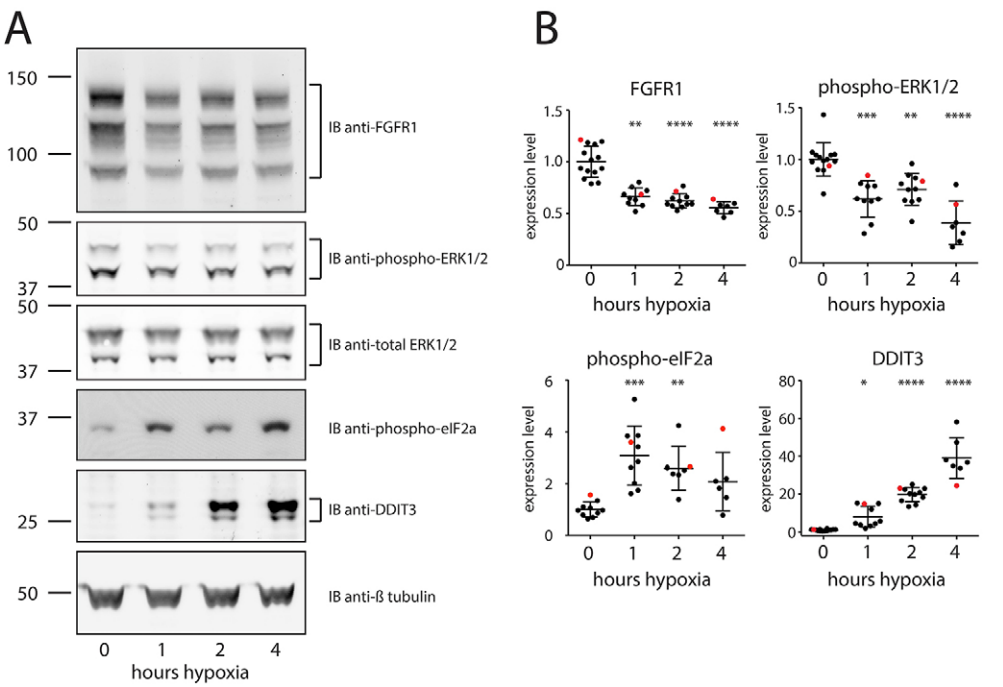

Fig. 5. Hypoxia induces the UPR and FGFR1 loss *in vitro*. (A) Representative immunoblots (IB) showing endogenous expression levels of FGFR1 (three bands representing fully glycosylated and partially glycosylated polypeptides), phospho-ERK1/2, total ERK1/2, phospho-EIF2α and DDIT3 in mouse muscle satellite C2C12 cells exposed to 0.1% oxygen for the indicated times. β-tubulin was used as a loading control. Molecular marker sizes are shown in kDa. (B) Quantification of expression levels of FGFR1, phospho-ERK1/2 (relative to total ERK1/2), phospho-EIF2α and DDIT3. Red dots indicate values for the immunoblots shown in A. **P*<0.05, ***P*<0.01, ****P*<0.001, *****P*<0.0001. See also Fig. S5.

We also tested the effects of other UPR-inducing stressors on FGFR1 stability *in vitro*. Short-term treatment of cells with hydrogen peroxide, increased temperature or high pH all reduced FGFR1 protein levels by a similar extent to hypoxic treatment (Fig. S5A-C). Phosphorylated EIF2α was induced in all cases, confirming UPR activation (data not shown). Thus, other cellular stressors that induce the UPR, including increased reactive oxygen species or hyperthermia, also result in reduced FGFR1 protein levels *in vitro*.

FGFR1 protein levels are reduced *in vitro* and *in vivo* due to UPR-triggered translation inhibition

The UPR involves three separate signaling pathways mediated by IRE1 (also known as ERN1), PERK (also known as EIF2AK3) and ATF6. We next investigated whether the reduction in FGFR1 protein levels *in vitro* is due to the action of one particular pathway. The UPR activates the IRE1 pathway via *Xbp1* transcript splicing, enabling translation of this transcription factor, increasing the expression of chaperones and activating the degradation of misfolded proteins. We compared FGFR1 protein levels in hypoxic cells with or without treatment with a small molecule inhibitor of IRE1, 4-methyl umbelliferone 8-carbaldehyde (4μ8c) (Cross et al., 2012). Hypoxia caused a significant reduction in FGFR1 protein levels, and treatment with 4μ8c did not alter this response (Fig. 6A). To confirm the efficacy of 4μ8c treatment, we monitored *Xbp1* splicing levels using the transiently transfected FLAG-XBP1ΔDBD-venus reporter (Iwawaki et al., 2004). As expected, hypoxia activated *Xbp1* splicing, and treatment with 4μ8c under hypoxic conditions prevented *Xbp1* splicing (Fig. 6B). We also confirmed the specificity of 4μ8c action, as induced levels of phosphorylated EIF2α and DDIT3 under hypoxic conditions were unaffected by 4μ8c treatment (Fig. 6C,D).

The UPR also causes a global reduction in cap-dependent translation. This process is controlled by activation of the serine-threonine kinase PERK, which phosphorylates and inactivates the translation initiation factor EIF2α (Kitamura, 2013). We compared FGFR1 and phosphorylated ERK1/2 protein levels in hypoxic cells with or without treatment with an inhibitor of PERK, GSK2606414 (Axten et al., 2012) (Fig. 6E,F). As above, we confirmed inhibitor activity and specificity by monitoring phosphorylated EIF2α and DDIT3 levels (Fig. 6G,H). Strikingly, treatment with GSK2606414 rescued the reduction in FGFR1 levels induced by hypoxia. This rescue of FGFR1 levels did not result in sustained phosphorylated ERK1/2. Three FGFR1 bands, with different degrees of glycosylation, were detected by immunoblotting (Fig. 6I). The highest molecular weight band (140 kDa), resistant to endoglycosidase H (EndoH) digestion, represents the mature form of FGFR1 (Fig. S5D) (Koika et al., 2013). Although total FGFR1 levels were rescued by GSK2606414 treatment (Fig. 6E), levels of the mature form of the receptor increased to a lesser extent than the immature forms (Fig. 6I-K). The abnormal buildup of the immature forms suggests that receptor maturation is disrupted by hypoxia, providing an explanation for why phosphorylated ERK1/2 levels were not rescued (Fig. 6F).

We next sought to confirm that FGFR1 levels could be rescued by inhibiting PERK in embryos exposed to hypoxia (Fig. 6L-O). We treated pregnant C57BL/6J mice on E9.5 with a single dose of GSK2606414 by oral gavage 1 h before exposure to 5.5% oxygen for 2 h. As before, low oxygen exposure without GSK2606414 treatment resulted in a significant loss of both total and Golgi-localized FGFR1 protein and, importantly, treatment with GSK2606414 rescued the hypoxia-induced reduction in FGFR1 in the SHF (Fig. 6T,U). Consistent with our *in vitro* findings, phosphorylated ERK1/2 levels were not sustained in the SHF despite normal FGFR1 levels (Fig. 6P-S,V).

These data indicate that inhibition of FGFR1 protein levels in response to hypoxia occurs specifically by PERK-induced inhibition of translation, both *in vitro* and *in vivo*. PERK inhibition restored FGFR1 levels generally, but not the mature active form of FGFR1 and, consequently, not signaling via phosphorylated ERK1/2.

DISCUSSION

Almost 200 years ago, Étienne Geoffroy Saint Hilaire showed that gestational hypoxia disrupts embryonic development (Geoffroy

Development (2016) 143, 2561-2572 doi:10.1242/dev.136820

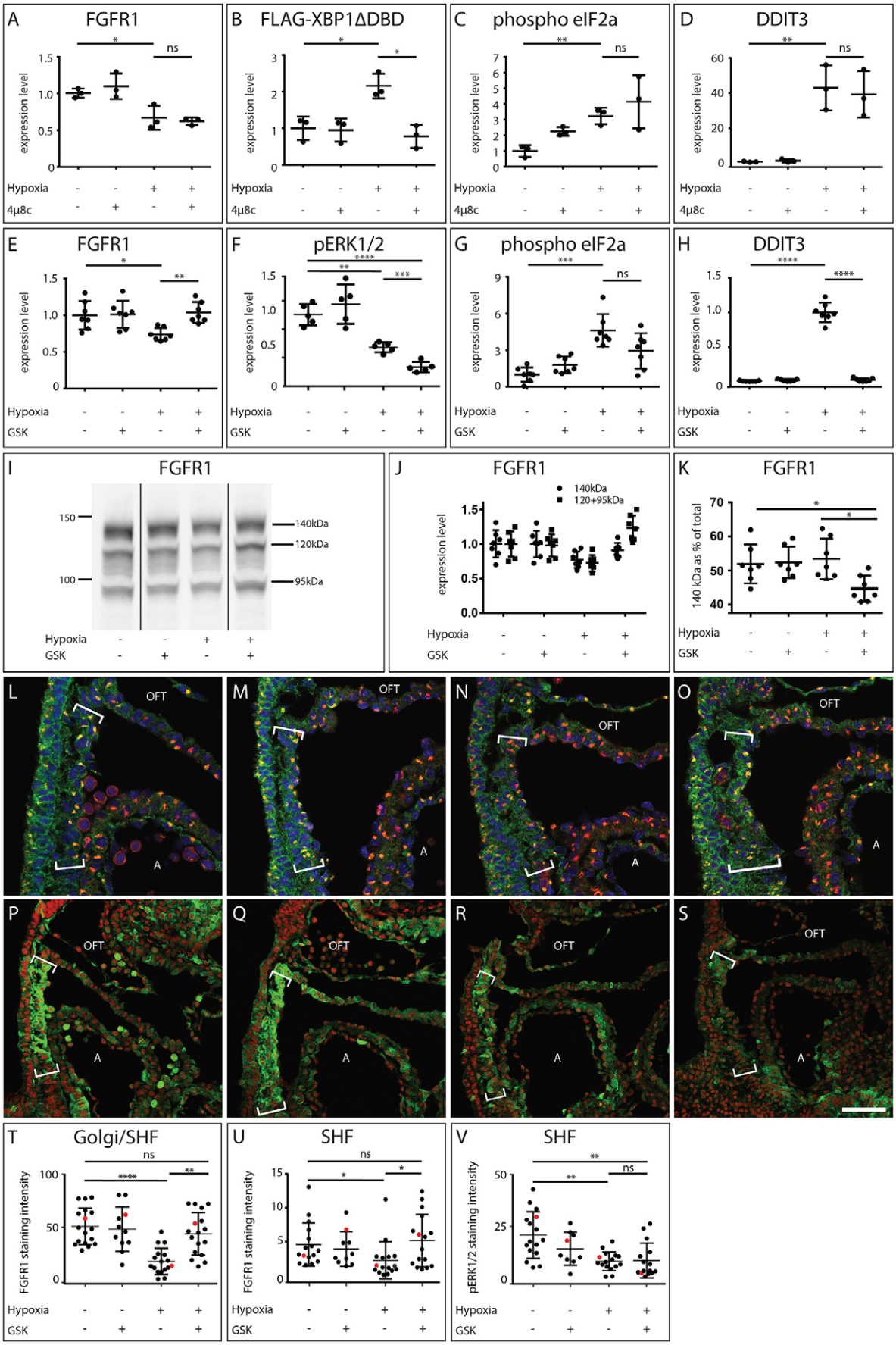

Fig. 6. See next page for legend.

Development (2016) 143, 2561-2572 doi:10.1242/dev.136820

Fig. 6. UPR-mediated translation inhibition mediates FGFR1 loss in response to hypoxic exposure *in vitro* and *in vivo*. (A-D) Quantification of expression levels of FGFR1, FLAG-XBP1ΔDBD, phospho-EIF2α and DDIT3 in C2C12 cells treated with 20 µM 4µ8c, an inhibitor of IRE1. (E-H) Quantification of the expression levels of FGFR1, phospho-ERK1/2, phospho-EIF2α and DDIT3 in C2C12 cells treated with 1 µM GSK2606414, an inhibitor of PERK. (I-K) The PERK inhibitor predominantly rescued the immature forms of the FGFR1. (I) Immunoblot of endogenous FGFR1 in C2C12 cells exposed to hypoxia (0.1% oxygen) and treated with 1 µM GSK2606414 (GSK). Three FGFR1 bands are detected, representing fully glycosylated (140 kDa) and partially glycosylated (120 kDa and 95 kDa) polypeptides. For clarity, irrelevant lanes were removed (vertical lines). (J) Quantification of the absolute levels of mature (circles) and immature (squares) forms of FGFR1. (K) Quantification of the mature, fully glycosylated FGFR1 polypeptide as a percentage of total FGFR1. (L-O) Comparison of FGFR1 (green) protein levels in unexposed and untreated control (L, *n*=17), unexposed and GSK26064414-treated (M, *n*=11), hypoxia-exposed and untreated (N, *n*=16) and hypoxia-exposed and GSK26064414-treated (O, *n*=17) embryos by immunohistochemistry on sagittal paraffin sections for FGFR1 (green) and GM130 (Golgi, red); nuclei were stained with TO-PRO-3 (blue). (P-S) Comparison of phospho-ERK1/2 (green) protein levels in unexposed and untreated control (P, *n*=16), unexposed and GSK26064414-treated (Q, *n*=9), hypoxia-exposed and untreated (R, *n*=16) and hypoxia-exposed and GSK26064414-treated (S, *n*=15) embryos by immunohistochemistry on sagittal paraffin sections for phospho-ERK1/2 (green); nuclei were stained with TO-PRO-3 (red). (T) Quantification of FGFR1 protein levels in the Golgi of the SHF. (U) Quantification of total FGFR1 protein levels in the SHF. (V) Quantification of phospho-ERK1/2 levels in the SHF. Red dots indicate values for the embryos shown in L-S. **P*<0.05, ***P*<0.01, ****P*<0.001, *****P*<0.0001; ns, not significant. Location of the SHF is indicated by brackets. Scale bar in S: 40 µm in L-O; 80 µm in P-S.

Saint Hilaire, 1820). The cellular and molecular consequences of this finding are only now being elucidated. We have previously shown that short-term gestational hypoxia disrupts FGF signaling in the PSM, altering somitogenesis and leading to vertebral defects (Sparrow et al., 2012). Here we extend this study by demonstrating that short-term gestational hypoxia causes abnormal heart development, resulting in heart defects that are the most common subtype of human CHD. Interestingly, we observed an almost bimodal response to hypoxia, with only ∼50% of embryos developing heart defects after hypoxic exposure. This supports the notion that the cause of some of the variation in the clinical outcome of human cases of CHD is environmental in nature. The defects induced by hypoxia are consistent with impaired function of a progenitor population of the heart, namely the SHF. Accordingly, we show that hypoxia reduces FGFR1 protein levels and FGF signaling in the SHF, and also activates the UPR. In both cultured cells and *in vivo*, we identify that the reduced levels of FGFR1 are likely to be caused by one specific function of the UPR: inhibition of cap-dependent translation. However, it should be noted that we were not able to test whether the third UPR pathway (mediated by ATF6) is also involved. We suggest a model in which the hypoxia-induced UPR results in reduced FGF signaling in the SHF, disrupting heart development and leading to morphological heart defects. We propose that other stressors that trigger the UPR during embryogenesis, such as increased reactive oxygen species or hyperthermia, may also cause CHD. In addition, UPR activation by such stressors may also occur in sites in addition to the SHF. This suggests that activation of the UPR might be a more general disruptor of embryogenesis and thus causes a range of birth defects.

Cells respond to stresses in a variety of ways, of which the UPR is only one. It is formally possible that other cellular stress responses are activated by hypoxia, such as the mTOR pathway (Wouters and Koritzinsky, 2008) and the nucleolar stress response (Boulon et al., 2010; James et al., 2014). The effects of these pathways on heart development could be assessed in future studies.

The hypoxia-mediated induction of the UPR is reversible in our mouse model. This is evident from the reiterative nature of somitogenesis, where each somite is independently formed temporally and spatially. Thus, somites formed after gestational hypoxia ceases are normal, and these give rise to normal vertebrae (Sparrow et al., 2012). By contrast, transient activation of the UPR has lasting morphological effects on the heart. This is because the final structure of the heart relies on many interdependent processes during embryogenesis, with perturbation at any point disrupting its final structure. Thus, although the UPR is reversible during embryogenesis, the effects on organ morphology can be enduring.

One of the early UPR responses is PERK-dependent attenuation of general protein synthesis. Therefore, it might be expected that a short-term translation block would simply cause a temporary reduction in embryo growth rate. However, the translation block appears to particularly affect the levels of some proteins but not others. In doing so, it disrupts specific processes and leads to distinct morphological defects. One explanation for this is that the UPR-induced translation block specifically affects cellular processes that are reliant on a rapid replenishment of proteins. For example, FGFR1-mediated signaling results in receptor degradation, and for signaling to continue more FGFR1 needs to be translated (Haugsten et al., 2005). Thus, FGFR1 cell surface replacement would be prevented by PERK-induced translation inhibition. This is in contrast to FGFR4, where receptor recycling, rather than degradation, occurs after activation. We might expect receptors of this type to be unaffected by translation inhibition. Indeed, this might explain why expression levels of PDGFRβ protein, another receptor tyrosine kinase expressed in the SHF, like FGFR1, were not affected by hypoxia within the experimental time frame. This differential effect of the UPR on receptor expression and function is an important area for future investigation.

We show that the hypoxia-induced reduction of FGFR1 is due to activation of the UPR and the PERK-dependent inhibition of translation. Inhibition of PERK rescued FGFR1 in cultured cells and *in vivo*, but did not rescue the reduction of phosphorylated ERK1/2. This can be explained by the fact that, although total FGFR1 levels are restored, the mature form of the receptor is significantly underrepresented. This is not surprising, as although GSK2606414 relieves the inhibition of translation, hypoxia would still inhibit protein folding and maturation in the ER and Golgi (Koritzinsky et al., 2013).

Potentially any stressor present during gestation that triggers the UPR in a tissue where FGFR1 is active could disrupt FGF-dependent developmental processes and lead to birth defects. Accordingly, our studies show that gestational hypoxia at E9.5 in mouse disrupts FGF signaling in the precursor tissues of the heart and vertebrae leading to defects in these structures (this study; Sparrow et al., 2012). The development of other organs might well be disrupted, as FGF/FGFR1 signaling has many key roles in embryogenesis (Thisse and Thisse, 2005; Itoh and Ornitz, 2011). More broadly, our findings suggest that any gestational stress that activates the UPR could disrupt any number of developmental processes and lead to birth defects. The types and numbers of defects that arise will be affected by the timing, duration and degree of the stress during embryogenesis, and the robustness of the developmental processes to withstand perturbation. In humans, different types of birth defects can arise with a non-random co-occurrence. For example, patients with a spectrum of various

Development (2016) 143, 2561-2572 doi:10.1242/dev.136820

combinations of 'vertebral anomalies, anal atresia, cardiac defects, tracheoesophageal fistula and/or esophageal atresia, renal and radial anomalies and limb defects' may be classified as having VACTERL association (OMIM 192350). It is possible that the critical stages of development of these organs are coincident. If so, activation of the UPR during this stage of embryogenesis might result in VACTERL.

How likely is it that the UPR is triggered during gestation? In addition to hypoxia, the UPR is activated in response to a variety of environmental stressors such as pollution and pathological conditions including maternal diabetes, viral infection and hyperthermia (Kitamura, 2013). Strikingly, many of these are identified as environmental risk factors for causing congenital malformation in humans (Jenkins et al., 2007). For example, offspring of mothers with pre-gestational diabetes have a significantly increased risk of CHD, with a relative risk of 3-18 (Jenkins et al., 2007), and the embryos of diabetic mice show significant activation of the UPR (Zhao, 2012). In addition, the stressors hyperthermia and hypoxemia are both associated with increased risk of birth defects in humans (Jenkins et al., 2007) and with activation of the UPR in cell culture (Kitamura, 2013). Thus, our results might provide a mechanism for the induction of birth defects by a wide array of environmental factors.

Finally, our *in vitro* system could be used as the basis of a high-throughput screening strategy to identify potential prophylactic agents to reduce the risks of CHD following the folate/neural tube defect paradigm (MRC Vitamin Study Research Group, 1991). Such prophylactic agents could then be validated in our *in vivo* system. This has an encouraging precedent, as oral treatment targeting the UPR abrogates the development of clinical prion disease in mice (Moreno et al., 2013). Such an approach has the potential to significantly reduce the incidence of human congenital defects.

MATERIALS AND METHODS

Animal experiments

All animal experiments were performed in accordance with protocols approved by the Garvan Institute of Medical Research/St Vincent's Animal Experimentation Ethics Committee, Sydney, Australia (approval 12/33). C57BL6/J dams and sires were mated. Pregnant mice were exposed to reduced oxygen levels at normal atmospheric pressure as described (Sparrow et al., 2012). After exposure, the mice were either sacrificed and embryos harvested, or mice were returned to normoxia for embryo harvest at a later date. For GSK2606414 experiments, pregnant mice were dosed with 50 mg/kg by oral gavage on E9.5, 1 h prior to hypoxic exposure. This dose was previously shown to effectively prevent UPR-mediated translational repression *in vivo* (Moreno et al., 2013).

Heart morphology

Heart morphology was determined using paraffin sectioning or magnetic resonance imaging (MRI) as previously described (O'Reilly et al., 2014), or by optical projection tomography (OPT) as described in the supplementary Materials and Methods. Heart morphology for all samples was assessed by the same observer, with classification of heart defects confirmed by an independent observer.

TUNEL staining and immunohistochemistry

Paraffin sections were labeled with digoxigenin using the ApopTag Fluorescein In Situ Apoptosis Detection Kit (Abcam). Labeled DNA fragments were detected by anti-digoxigenin-alkaline phosphatase, Fab fragments (Roche Life Sciences) and NBT/BCIP solution (Roche Life Sciences). We performed whole-mount immunofluorescence on fixed embryos and sections as previously described (Geffers et al., 2007; Moreau et al., 2014). For details of immunohistochemistry, including quantitation methods, see the supplementary Materials and Methods and Table S2.

RNA *in situ* hybridization

We performed RNA whole-mount *in situ* hybridization as described previously (Dunwoodie et al., 1997) using the probes listed in the supplementary Materials and Methods.

Quantitative RT-PCR

Levels of spliced and unspliced *Xbp1* transcripts in RNA extracts from E9.5 whole embryos were determined using custom TaqMan gene expression assays (Applied Biosystems) designed using published sequences (Hayashi et al., 2007). RNA extraction, reverse transcription and qPCR were performed as previously described (O'Reilly et al., 2014).

Cell culture and immunoblot

Mouse muscle satellite C2C12 cells were cultured in low oxygen using an H35 Hypoxystation (Don Whitley Scientific). Culture medium was equilibrated in 0.1% oxygen overnight prior to use. Culture dishes were transferred to the workstation, rinsed once with hypoxia-equilibrated medium, and incubated in fresh hypoxia-equilibrated medium for the indicated times. For the study of UPR inhibitors, cells were incubated for 2 h in normoxic or hypoxia-equilibrated medium containing inhibitor. For detection of *Xbp1* splicing in the 4μ8c experiments, a plasmid encoding FLAG-tagged XBP1ΔDBD-venus (Iwawaki et al., 2004) was transiently transfected into C2C12 cells using Lipofectamine LTX and PLUS reagent (Life Technologies) 24 h prior to hypoxic exposure. For further details, see the supplementary Materials and Methods.

Statistical analyses

All statistical analyses were performed with Prism 6 (GraphPad Software). Gene and protein staining intensity from RNA whole-mount *in situ* hybridizations, immunohistochemistry and immunoblot experiments were compared using Kruskal–Wallis one-way ANOVA with Dunnett's post-hoc test to compare all treatment groups with the control, except for the data in Fig. 4L and Fig. 6A-J, which were tested with ANOVA followed by Tukey's post-hoc test to compare the means of each group with every other group. The linear correlation between distal OFT length and the inner angle between proximal and distal OFT (Fig. 1) was tested using non-parametric Spearman correlation. The statistical significance of the prevalence of heart defects or resorbed embryos in exposed versus unexposed embryos (Table 1) was tested using a one-tailed Fisher's exact test. In figures, data are presented as mean±s.d.

Acknowledgements

We thank G. Martin, I. Mason and M. Muira for plasmids; BioCORE staff and Y. Wang for technical assistance; G. Maghzal for technical and intellectual assistance; Herbert Smith for donating the confocal microscopes and Chain Reaction for donating the OPT used in this study. We remember B. E. Chapman (1948-2014) and his important contribution to this research.

Competing interests

The authors declare no competing or financial interests.

Author contributions

H.S., V.C.O., J.L.M.M., T.R.B., M.X.Y., B.E.C., S.M.G., G.C. and D.B.S. performed experiments; H.S., V.C.O., J.L.M.M., T.R.B., M.X.Y., G.C., D.B.S., R.S. and S.L.D. analyzed data; H.S., R.S., R.M.G., G.C., D.B.S. and S.L.D. wrote the manuscript; S.M.G., R.S., R.M.G., D.B.S. and S.L.D. secured funding; S.L.D. conceived the study and is responsible for all aspects of this research and its communication.

Funding

This research was supported by the National Health and Medical Research Council (NHMRC) [project grant ID 1019776 to S.L.D., D.B.S. and S.M.G.; program grant ID 1074386 to R.M.G. and S.L.D.; and Senior Research Fellowship ID 1042002 to S.L.D.]; Chain Reaction (The Ultimate Corporate Bike Challenge); and the Office of Health and Medical Research, NSW State Government (R.M.G., S.L.D. and R.S.).

Supplementary information

Supplementary information available online at
http://dev.biologists.org/lookup/doi/10.1242/dev.136820.supplemental

Development (2016) 143, 2561-2572 doi:10.1242/dev.136820

References

Abu-Issa, R., Smyth, G., Smoak, I., Yamamura, K. and Meyers, E. N. (2002). Fgf8 is required for pharyngeal arch and cardiovascular development in the mouse. *Development* **129**, 4613-4625.

Andersen, T. A., Troelsen, K. d. L. L. and Larsen, L. A. (2014). Of mice and men: molecular genetics of congenital heart disease. *Cell. Mol. Life Sci.* **71**, 1327-1352.

Axten, J. M., Medina, J. R., Feng, Y., Shu, A., Romeril, S. P., Grant, S. W., Li, W. H. H., Heerding, D. A., Minthorn, E., Mencken, T. et al. (2012). Discovery of 7-methyl-5-(1-{[3-(trifluoromethyl)phenyl]acetyl}-2,3-dihydro-1H-indol-5-yl)-7H-pyrrolo[2,3-d]pyrimidin-4-amine (GSK2606414), a potent and selective first-in-class inhibitor of protein kinase R (PKR)-like endoplasmic reticulum kinase (PERK). *J. Med. Chem.* **55**, 7193-7207.

Benson, D. W., Silberbach, G. M., Kavanaugh-McHugh, A., Cottrill, C., Zhang, Y., Riggs, S., Smalls, O., Johnson, M. C., Watson, M. S., Seidman, J. G. et al. (1999). Mutations in the cardiac transcription factor NKX2.5 affect diverse cardiac developmental pathways. *J. Clin. Invest.* **104**, 1567-1573.

Blue, G. M., Kirk, E. P., Sholler, G. F., Harvey, R. P. and Winlaw, D. S. (2012). Congenital heart disease: current knowledge about causes and inheritance. *Med. J. Aust.* **197**, 155-159.

Boulon, S., Westman, B. J., Hutten, S., Boisvert, F. M. and Lamond, A. I. (2010). The nucleolus under stress. *Mol. Cell* **40**, 216-227.

Brown, C. B., Wenning, J. M., Lu, M. M., Epstein, D. J., Meyers, E. N. and Epstein, J. A. (2004). Cre-mediated excision of Fgf8 in the Tbx1 expression domain reveals a critical role for Fgf8 in cardiovascular development in the mouse. *Dev. Biol.* **267**, 190-202.

Bruneau, B. G. (2008). The developmental genetics of congenital heart disease. *Nature* **451**, 943-948.

Cross, B. C. S., Bond, P. J., Sadowski, P. G., Jha, B. K., Zak, J., Goodman, J. M., Silverman, R. H., Neubert, T. A., Baxendale, I. R., Ron, D. et al. (2012). The molecular basis for selective inhibition of unconventional mRNA splicing by an IRE1-binding small molecule. *Proc. Natl. Acad. Sci. USA* **109**, E869-E878.

Dorey, K. and Amaya, E. (2010). FGF signalling: diverse roles during early vertebrate embryogenesis. *Development* **137**, 3731-3742.

Dunwoodie, S. L. (2009). The role of hypoxia in development of the Mammalian embryo. *Dev. Cell* **17**, 755-773.

Dunwoodie, S. L., Henrique, D., Harrison, S. M. and Beddington, R. S. (1997). Mouse Dll3: a novel divergent Delta gene which may complement the function of other Delta homologues during early pattern formation in the mouse embryo. *Development* **124**, 3065-3076.

Erck, C., Meisinger, C., Grothe, C. and Seidl, K. (1998). Regulation of nerve growth factor and its low-affinity receptor (p75NTR) during myogenic differentiation. *J. Cell. Physiol.* **176**, 22-31.

Fahed, A. C., Gelb, B. D., Seidman, J. G. and Seidman, C. E. (2013). Genetics of congenital heart disease: the glass half empty. *Circ. Res.* **112**, 707-720.

Feldman, D. E., Chauhan, V. and Koong, A. C. (2005). The unfolded protein response: a novel component of the hypoxic stress response in tumors. *Mol. Cancer Res.* **3**, 597-605.

Geffers, I., Serth, K., Chapman, G., Jaekel, R., Schuster-Gossler, K., Cordes, R., Sparrow, D. B., Kremmer, E., Dunwoodie, S. L., Klein, T., et al. (2007). Divergent functions and distinct localization of the Notch ligands DLL1 and DLL3 in vivo. *J. Cell Biol.* **178**, 465-476.

Geoffroy Saint Hilaire, E. (1820). Différents états de pesanteur des oeufs au commencement et a la fin de l'incubation. *J. Complemen. Sci. Med.* **7**, 271.

Haugsten, E. M., Sørensen, V., Brech, A., Olsnes, S. and Wesche, J. (2005). Different intracellular trafficking of FGF1 endocytosed by the four homologous FGF receptors. *J. Cell Sci.* **118**, 3869-3881.

Hayashi, A., Kasahara, T., Iwamoto, K., Ishiwata, M., Kametani, M., Kakiuchi, C., Furuichi, T. and Kato, T. (2007). The role of brain-derived neurotrophic factor (BDNF)-induced XBP1 splicing during brain development. *J. Biol. Chem.* **282**, 34525-34534.

Hutson, M. R., Zhang, P., Stadt, H. A., Sato, A. K., Li, Y.-X., Burch, J., Creazzo, T. L. and Kirby, M. L. (2006). Cardiac arterial pole alignment is sensitive to FGF8 signaling in the pharynx. *Dev. Biol.* **295**, 486-497.

Ilagan, R., Abu-Issa, R., Brown, D., Yang, Y.-P., Jiao, K., Schwartz, R. J., Klingensmith, J. and Meyers, E. N. (2006). Fgf8 is required for anterior heart field development. *Development* **133**, 2435-2445.

Ingalls, T. H., Curley, F. J. and Prindle, R. A. (1952). Experimental production of congenital anomalies; timing and degree of anoxia as factors causing fetal deaths and congenital anomalies in the mouse. *N. Engl. J. Med.* **247**, 758-768.

Itoh, N. and Ornitz, D. M. (2011). Fibroblast growth factors: from molecular evolution to roles in development, metabolism and disease. *J. Biochem.* **149**, 121-130.

Iwawaki, T., Akai, R., Kohno, K. and Miura, M. (2004). A transgenic mouse model for monitoring endoplasmic reticulum stress. *Nat. Med.* **10**, 98-102.

James, A., Wang, Y., Raje, H., Rosby, R. and DiMario, P. (2014). Nucleolar stress with and without p53. *Nucleus* **5**, 402-426.

Jenkins, K. J., Correa, A., Feinstein, J. A., Botto, L., Britt, A. E., Daniels, S. R., Elixson, M., Warnes, C. A., Webb, C. L. and American Heart Association Council on Cardiovascular Disease in the Young. (2007). Noninherited risk factors and congenital cardiovascular defects: current knowledge: a scientific statement from the American Heart Association Council on Cardiovascular Disease in the Young: endorsed by the American Academy of Pediatrics. *Circulation* **115**, 2995-3014.

Jiang, B. H., Semenza, G. L., Bauer, C. and Marti, H. H. (1996). Hypoxia-inducible factor 1 levels vary exponentially over a physiologically relevant range of O_2 tension. *Am. J. Physiol.* **271**, C1172-C1180.

Jukkola, T., Lahti, L., Naserke, T., Wurst, W. and Partanen, J. (2006). FGF regulated gene-expression and neuronal differentiation in the developing midbrain-hindbrain region. *Dev. Biol.* **297**, 141-157.

Kelly, R. G. (2012). The second heart field. *Curr. Top. Dev. Biol.* **100**, 33-65.

Kitamura, M. (2013). The unfolded protein response triggered by environmental factors. *Semin. Immunopathol.* **35**, 259-275.

Koika, V., Varnavas, P., Valavani, H., Sidis, Y., Plummer, L., Dwyer, A., Quinton, R., Kanaka-Gantenbein, C., Pitteloud, N., Sertedaki, A. et al. (2013). Comparative functional analysis of two fibroblast growth factor receptor 1 (FGFR1) mutations affecting the same residue (R254W and R254Q) in isolated hypogonadotropic hypogonadism (IHH). *Gene* **516**, 146-151.

Koritzinsky, M., Levitin, F., van den Beucken, T., Rumantir, R. A., Harding, N. J., Chu, K. C., Boutros, P. C., Braakman, I. and Wouters, B. G. (2013). Two phases of disulfide bond formation have differing requirements for oxygen. *J. Cell Biol.* **203**, 615-627.

Liao, J., Aggarwal, V. S., Nowotschin, S., Bondarev, A., Lipner, S. and Morrow, B. E. (2008). Identification of downstream genetic pathways of Tbx1 in the second heart field. *Dev. Biol.* **316**, 524-537.

Marguerie, A., Bajolle, F., Zaffran, S., Brown, N. A., Dickson, C., Buckingham, M. E. and Kelly, R. G. (2006). Congenital heart defects in Fgfr2-IIIb and Fgf10 mutant mice. *Cardiovasc. Res.* **71**, 50-60.

Miquerol, L. and Kelly, R. G. (2013). Organogenesis of the vertebrate heart. *Wiley Interdiscip. Rev. Dev. Biol.* **2**, 17-29.

Moreau, J. L. M., Artap, S. T., Shi, H., Chapman, G., Leone, G., Sparrow, D. B. and Dunwoodie, S. L. (2014). Cited2 is required in trophoblasts for correct placental capillary patterning. *Dev. Biol.* **392**, 62-79.

Moreno, J. A., Halliday, M., Molloy, C., Radford, H., Verity, N., Axten, J. M., Ortori, C. A., Willis, A. E., Fischer, P. M., Barrett, D. A. et al. (2013). Oral treatment targeting the unfolded protein response prevents neurodegeneration and clinical disease in prion-infected mice. *Sci. Transl. Med.* **5**, 206ra138.

MRC Vitamin Study Research Group (1991). Prevention of neural tube defects: results of the Medical Research Council Vitamin Study. *Lancet* **338**, 131-137.

Neeb, Z., Lajiness, J. D., Bolanis, E. and Conway, S. J. (2013). Cardiac outflow tract anomalies. *Wiley Interdiscip. Rev. Dev. Biol.* **2**, 499-530.

O'Reilly, V. C., Lopes Floro, K., Shi, H., Chapman, B. E., Preis, J. I., James, A. C., Chapman, G., Harvey, R. P., Johnson, R. S., Grieve, S. M. et al. (2014). Gene-environment interaction demonstrates the vulnerability of the embryonic heart. *Dev. Biol.* **391**, 99-110.

Ornoy, A., Reece, E. A., Pavlinkova, G., Kappen, C. and Miller, R. K. (2015). Effect of maternal diabetes on the embryo, fetus, and children: congenital anomalies, genetic and epigenetic changes and developmental outcomes. *Birth Defects Res. C Embryo Today* **105**, 53-72.

Ozaki, S., Radeke, M. J. and Anderson, D. H. (2000). Rapid upregulation of fibroblast growth factor receptor 1 (flg) by rat photoreceptor cells after injury. *Invest. Ophthalmol. Vis. Sci.* **41**, 568-579.

Park, E. J., Ogden, L. A., Talbot, A., Evans, S., Cai, C.-L., Black, B. L., Frank, D. U. and Moon, A. M. (2006). Required, tissue-specific roles for Fgf8 in outflow tract formation and remodeling. *Development* **133**, 2419-2433.

Park, E. J., Watanabe, Y., Smyth, G., Miyagawa-Tomita, S., Meyers, E., Klingensmith, J., Camenisch, T., Buckingham, M. and Moon, A. M. (2008). An FGF autocrine loop initiated in second heart field mesoderm regulates morphogenesis at the arterial pole of the heart. *Development* **135**, 3599-3610.

Prudovsky, I., Savion, N., Zhan, X., Friesel, R., Xu, J., Hou, J., McKeehan, W. L. and Maciag, T. (1994). Intact and functional fibroblast growth factor (FGF) receptor-1 trafficks near the nucleus in response to FGF-1. *J. Biol. Chem.* **269**, 31720-31724.

Raleigh, J. A., Chou, S.-C., Arteel, G. E. and Horsman, M. R. (1999). Comparisons among pimonidazole binding, oxygen electrode measurements, and radiation response in C3H mouse tumors. *Radiat. Res.* **151**, 580-589.

Ramakrishnan, A., Lee, L. J., Mitchell, L. E. and Agopian, A. J. (2015). Maternal hypertension during pregnancy and the risk of congenital heart defects in offspring: a systematic review and meta-analysis. *Pediatr. Cardiol.* **36**, 1442-1451.

Schott, J.-J., Benson, D. W., Basson, C. T., Pease, W., Silberbach, G. M., Moak, J. P., Maron, B. J., Seidman, C. E. and Seidman, J. G. (1998). Congenital heart disease caused by mutations in the transcription factor NKX2-5. *Science* **281**, 108-111.

Sparrow, D. B., Chapman, G., Smith, A. J., Mattar, M. Z., Major, J. A., O'Reilly, V. C., Saga, Y., Zackai, E. H., Dormans, J. P., Alman, B. A. et al. (2012). A mechanism for gene-environment interaction in the etiology of congenital scoliosis. *Cell* **149**, 295-306.

Sullivan, P. M., Dervan, L. A., Reiger, S., Buddhe, S. and Schwartz, S. M. (2015). Risk of congenital heart defects in the offspring of smoking mothers: a population-based study. *J. Pediatr.* **166**, 978-984 e2.

Thisse, B. and Thisse, C. (2005). Functions and regulations of fibroblast growth factor signaling during embryonic development. *Dev. Biol.* **287**, 390-402.

Development (2016) 143, 2561-2572 doi:10.1242/dev.136820

Thom, T., Haase, N., Rosamond, W., Howard, V. J., Rumsfeld, J., Manolio, T., Zheng, Z. J., Flegal, K., O'Donnell, C., Kittner, S. et al. (2006). Heart disease and stroke statistics–2006 update: a report from the American Heart Association Statistics Committee and Stroke Statistics Subcommittee. *Circulation* **113**, e85-e151.

van der Linde, D., Konings, E. E. M., Slager, M. A., Witsenburg, M., Helbing, W. A., Takkenberg, J. J. M. and Roos-Hesselink, J. W. (2011). Birth prevalence of congenital heart disease worldwide: a systematic review and meta-analysis. *J. Am. Coll. Cardiol.* **58**, 2241-2247.

Wang, G. L., Jiang, B. H., Rue, E. A. and Semenza, G. L. (1995). Hypoxia-inducible factor 1 is a basic-helix-loop-helix-PAS heterodimer regulated by cellular O_2 tension. *Proc. Natl. Acad. Sci. USA* **92**, 5510-5514.

Watanabe, Y., Miyagawa-Tomita, S., Vincent, S. D., Kelly, R. G., Moon, A. M. and Buckingham, M. E. (2010). Role of mesodermal FGF8 and FGF10 overlaps in the development of the arterial pole of the heart and pharyngeal arch arteries. *Circ. Res.* **106**, 495-503.

Watkins, M. L., Rasmussen, S. A., Honein, M. A., Botto, L. D. and Moore, C. A. (2003). Maternal obesity and risk for birth defects. *Pediatrics* **111**, 1152–1158.

Webster, W. S., Nilsson, M. and Ritchie, H. (2014). Therapeutic drugs that slow the heart rate of early rat embryos. Is there a risk for the human? *Curr. Pharm. Des* **20**, 5364-5376.

Wouters, B. G. and Koritzinsky, M. (2008). Hypoxia signalling through mTOR and the unfolded protein response in cancer. *Nat. Rev. Cancer* **8**, 851-864.

Xu, H., Morishima, M., Wylie, J. N., Schwartz, R. J., Bruneau, B. G., Lindsay, E. A. and Baldini, A. (2004). Tbx1 has a dual role in the morphogenesis of the cardiac outflow tract. *Development* **131**, 3217-3227.

Zhang, J., Lin, Y., Zhang, Y., Lan, Y., Lin, C., Moon, A. M., Schwartz, R. J., Martin, J. F. and Wang, F. (2008). Frs2alpha-deficiency in cardiac progenitors disrupts a subset of FGF signals required for outflow tract morphogenesis. *Development* **135**, 3611-3622.

Zhao, Z. (2012). Endoplasmic reticulum stress in maternal diabetes-induced cardiac malformations during critical cardiogenesis period. *Birth Defects Res. B Dev. Reprod. Toxicol.* **95**, 1-6.

Zheng, J.-Y., Tian, H.-T., Zhu, Z.-M., Li, B., Han, L., Jiang, S.-L., Chen, Y., Li, D.-T., He, J.-C., Zhao, Z. et al. (2013). Prevalence of symptomatic congenital heart disease in Tibetan school children. *Am. J. Cardiol.* **112**, 1468-1470.

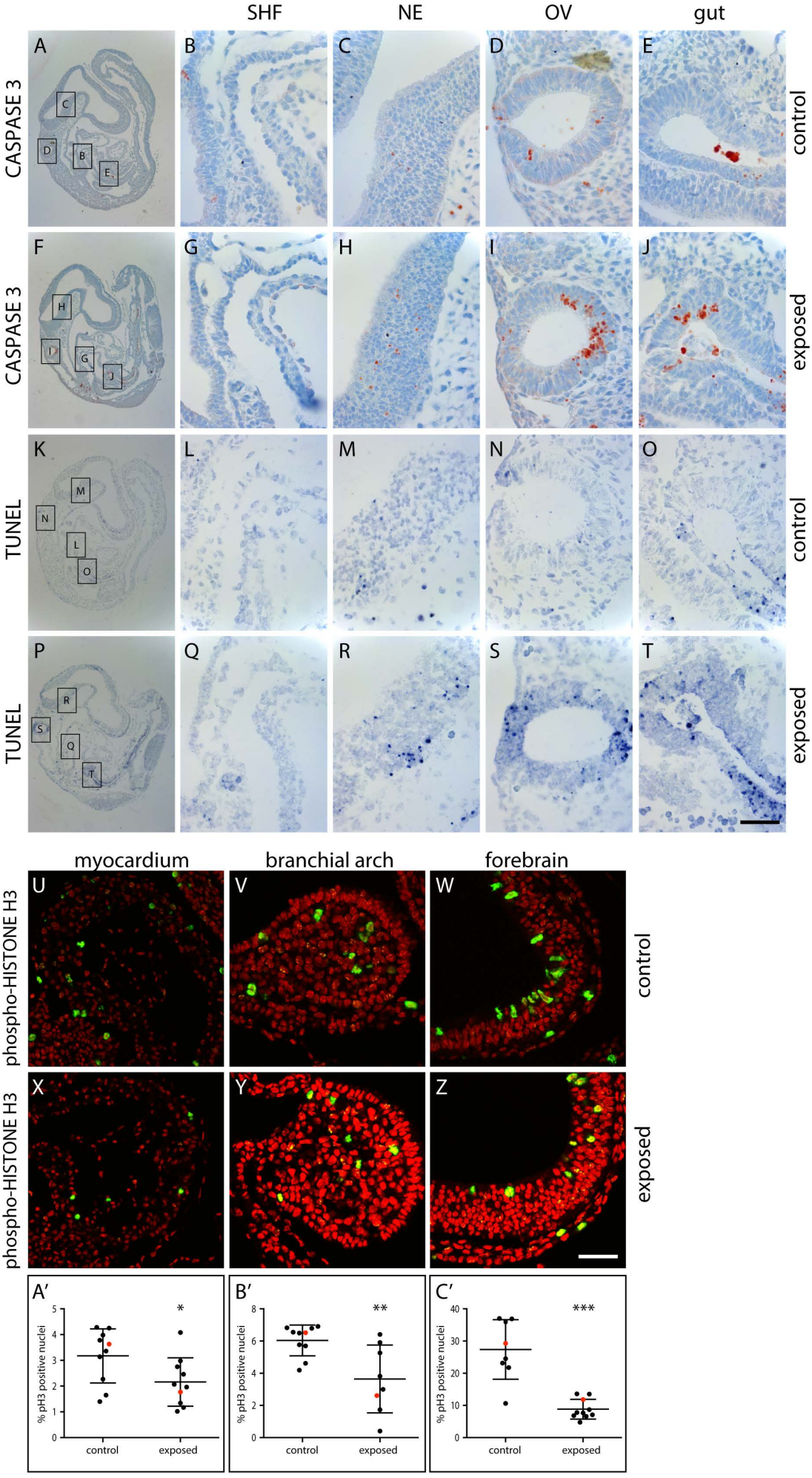

Figure S1. Effects of Low Oxygen Exposure of E9.5 Mouse Embryos on Apoptosis and Proliferation of Second Heart Field Cells. Related to Figure 1.
(A-J) Comparison of active/pro Caspase 3 protein levels (red) in control (A-E, n=10) and exposed (8 hours, F-J, n=10) E9.5 mouse embryos using immunohistochemistry on sagittal paraffin sections. (A and F) Low magnification images of representative sections. (B-E and G-J) High magnification images of the boxed regions of panels A and F showing the second heart field (SHF), neuroectoderm (NE), otic vesicle (OV) and gut. Sections were counterstained with haemotoxylin (light blue). (K-T) Comparison of TUNEL staining (dark blue) on adjacent sagittal paraffin sections of control (K-O, n=10) and exposed (P-T, n=10) E9.5 mouse embryos. (K and P) Low magnification images of representative sections. (L-O and Q-T) High magnification images of the boxed regions of panels K and P showing the second heart field (SHF), neuroectoderm (NE), otic vesicle (OV) and gut. (U-C') Comparison of phospho- histone H3 protein levels (green) in control (U-W, n=10) and exposed (X-Z, n=10) E9.5 mouse embryos using immunohistochemistry on sagittal paraffin sections. Nuclei were stained with TO- PRO-3 (red). Representative sections of myocardium (U,X), branchial arch (V,Y) and forebrain (W,Z) are shown. (A'-C') Quantification of percentage of phospho-histone H3 positive nuclei for each tissue. Red dots indicate the quantification of the images shown in panels (U-Z). Scale bars: 560 μm (A, F, K and P), 70 μm (B-E, G-J, L-O and Q-T), 110 μm (U,X) and 50 μm (V,W,Y,Z). Graph shows mean and standard deviation. * $p<0.05$, ** $p<0.01$, *** $p<0.001$

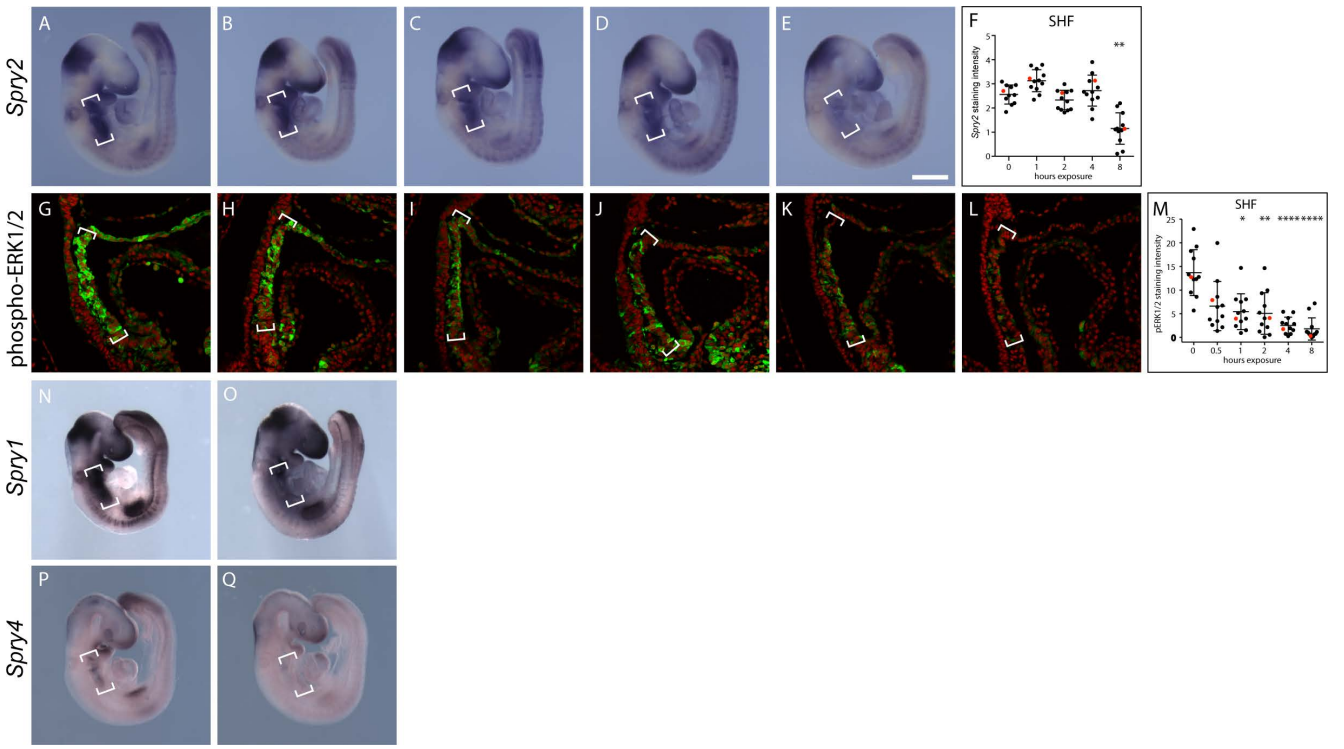

Figure S2. Effects of Low Oxygen Exposure of E9.5 Mouse Embryos on FGF Signaling Targets in the Second Heart Field. Related to Figure 2.

(A-F) Comparison of gene expression levels of Spry2 in control (A, n=11) and exposed (B-E) E9.5 mouse embryos using whole-mount RNA in situ hybridization. Exposure times in hours were 1 (B, n=12), 2 (C, n=12), 4 (D, n=12) and 8 (E, n=12). (F) Quantification of levels of Spry2 transcript in the second heart field (SHF). Red dots indicate the values for the embryos depicted in panels A-E. (G-M) Comparison of phospho-ERK1/2 (green) protein levels in control (G, n=12) and low oxygen exposed (H-L) E9.5 mouse embryos using immunohistochemistry on sagittal paraffin sections. Exposure times in hours were 0.5 (H, n=12), 1 (I, n=12), 2 (J, n=12), 4 (K, n=12) and 8 (L, n=12). Nuclei were stained with TO-PRO-3 (red). (M) Quantification of levels of phospho-ERK1/2 in the SHF. Red dots indicate the values for the embryos depicted in panels G-L. (N-O) Comparison of gene expression levels of Spry1 in control (N, n=5) and 8 hour exposed (O, n=5) E9.5 mouse embryos using whole-mount RNA in situ hybridization. (P-Q) Comparison of gene expression levels of Spry4 in control (P, n=12) and 8 hour exposed (Q, n=14) E9.5 mouse embryos using whole-mount RNA in situ hybridization. In panels showing sections, rostral is to the top and caudal to the bottom. Location of the SHF is indicated by brackets. OFT = outflow tract, v = ventricle, a = atrium. Scale bars: 500 μm (A-E, N-Q) and 40 μm (G-L). Graph shows mean and standard deviation. * $p < 0.05$, ** $p < 0.01$, **** $p < 0.0001$.

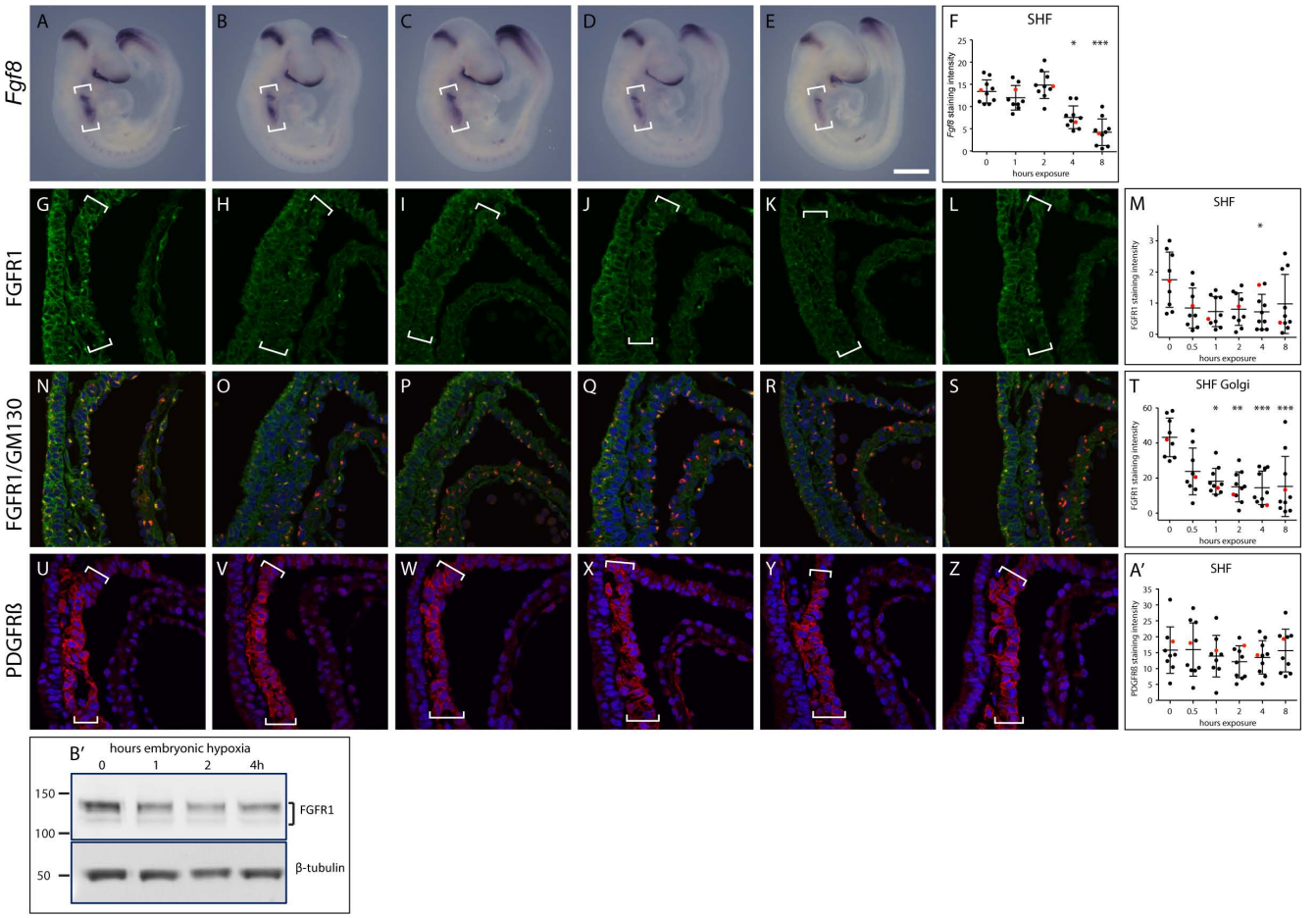

Figure S3. Effects of Low Oxygen Exposure of E9.5 Mouse Embryos on FGF Signaling Components in the Second Heart Field. Related to Figure 3.

(A-F) Comparison of gene expression levels of Fgf8 in control (A, n=10) and exposed (B-E) E9.5 mouse embryos using whole-mount RNA in situ hybridization. Exposure times in hours were 1 (B, n=9), 2 (C, n=10), 4 (D, n=10) and 8 (E, n=10). (F) Quantification of levels of Fgf8 transcript in the SHF. Red dots indicate the values for the embryos depicted in panels A-E. (G-M) Comparison of FGFR1 (green) protein levels in control (G, n=9) and low oxygen exposed (H-L) E9.5 mouse embryos using immunohistochemistry on sagittal paraffin sections. Exposure times in hours were 0.5 (H, n=9), 1 (I, n=10), 2 (J, n=10), 4 (K, n=10) and 8 (L, n=10). (M) Quantification of total levels of FGFR1 in the SHF. Red dots indicate the values for the embryos depicted in panels H-M. (N-S) Comparison of FGFR1 (green) protein levels in the Golgi of control (N, n=9) and low oxygen exposed (O- S) E9.5 mouse embryos using immunohistochemistry on sagittal paraffin sections. N-S are the same as G-L with the inclusion of staining for Golgi with GM130 (red) and nuclei with TO-PRO-3 (blue). (T) Quantification of levels of FGFR1 in SHF Golgi. Red dots indicate the values for the embryos depicted in panels N-S. (U-A') Comparison of PDGFRß (red) protein levels in control (U, n=9) and low oxygen exposed (W-Z) E9.5 mouse embryos using immunohistochemistry on sagittal paraffin sections. Exposure times in hours were 0.5 (V, n=10), 1 (W, n=9), 2 (X, n=10), 4 (Y, n=10) and 8 (Z, n=10). Nuclei were stained with TO-PRO-3 (blue). (A') Quantification of PDGFRß protein levels in the SHF. Red dots indicate the values for the embryos depicted in panels V-A'. (B') Example immunoblot showing total protein levels of FGFR1 in whole E9.5 embryos exposed to normoxia (0 hours), or 5.5% oxygen for 1-4 hours. Scale bars: 500 µm (A-E) and 40 µm (G-L, N-S and U-Z). In panels showing sections, rostral is to the top and caudal to the bottom. Location of the SHF is indicated by brackets. OFT = outflow tract, v = ventricle, a = atrium. Graph shows mean and standard deviation. * $p<0.05$, ** $p<0.01$, *** $p<0.001$.

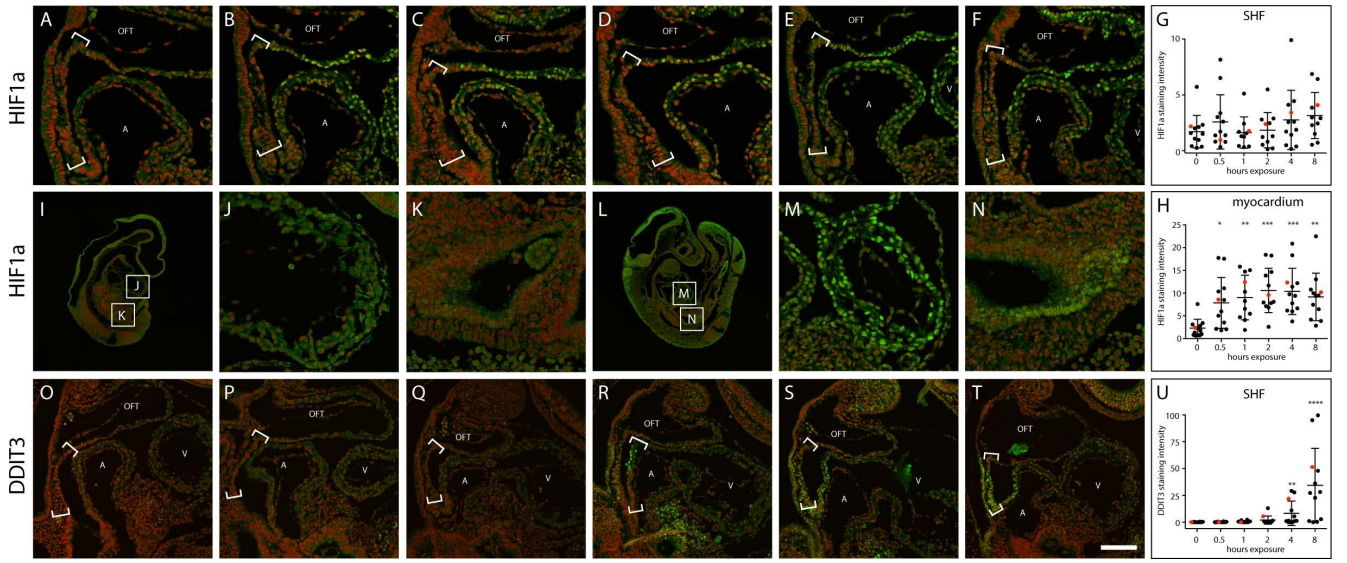

Figure S4. Cells in Embryos Exposed to Lowered Oxygen Levels in utero are Hypoxic and Induce the Unfolded Protein Response. Related to Figure 4.

(A-H) Comparison of HIF1α (green) protein levels in control (A, n=12) and exposed (B-F) E9.5 mouse embryos using immunohistochemistry on sagittal paraffin sections. Exposure times in hours were 0.5 (B, n=12), 1 (C, n=10), 2 (D, n=11), 4 (E, n=12) and 8 (F, n=11). Nuclei were stained with TO-PRO-3 (red). (G-H) Quantification of levels of HIF1α in the SHF (G) and myocardium (H). Red dots indicate the values for the embryos depicted in panels A-F. (I-N) Comparison of HIF1α (green) protein levels in control (I) and low oxygen exposed (L) E9.5 mouse embryos. Magnified views of the boxed areas in panels I and L showing HIF1α staining in myocardium (J and M) and gut (K and N). (O-U) Comparison of DDIT3 (green) protein levels in control (O, n=12) and low oxygen exposed (P-T) E9.5 mouse embryos using immunohistochemistry on sagittal paraffin sections. Exposure times in hours were 0.5 (P, n=12), 1 (Q, n=12), 2 (R, n=12), 4 (S, n=12) and 8 (T, n=12). Nuclei were stained with TO-PRO-3 (red). (U) Quantification of levels of DDIT3 in the SHF. Red dots indicate the values for the embryos depicted in panels O-T. In panels showing sections, rostral is to the top and caudal to the bottom. Scale bars: 80 μm (A-F), 570 μm (I and L), 70 μm (J-K, M- N) and 140 μm (O-T). Location of the SHF is indicated by brackets. OFT = outflow tract, v = ventricle, a = atrium. Graph shows mean and standard deviation. * $p<0.05$, ** $p<0.01$, *** $p<0.001$, **** $p<0.0001$.

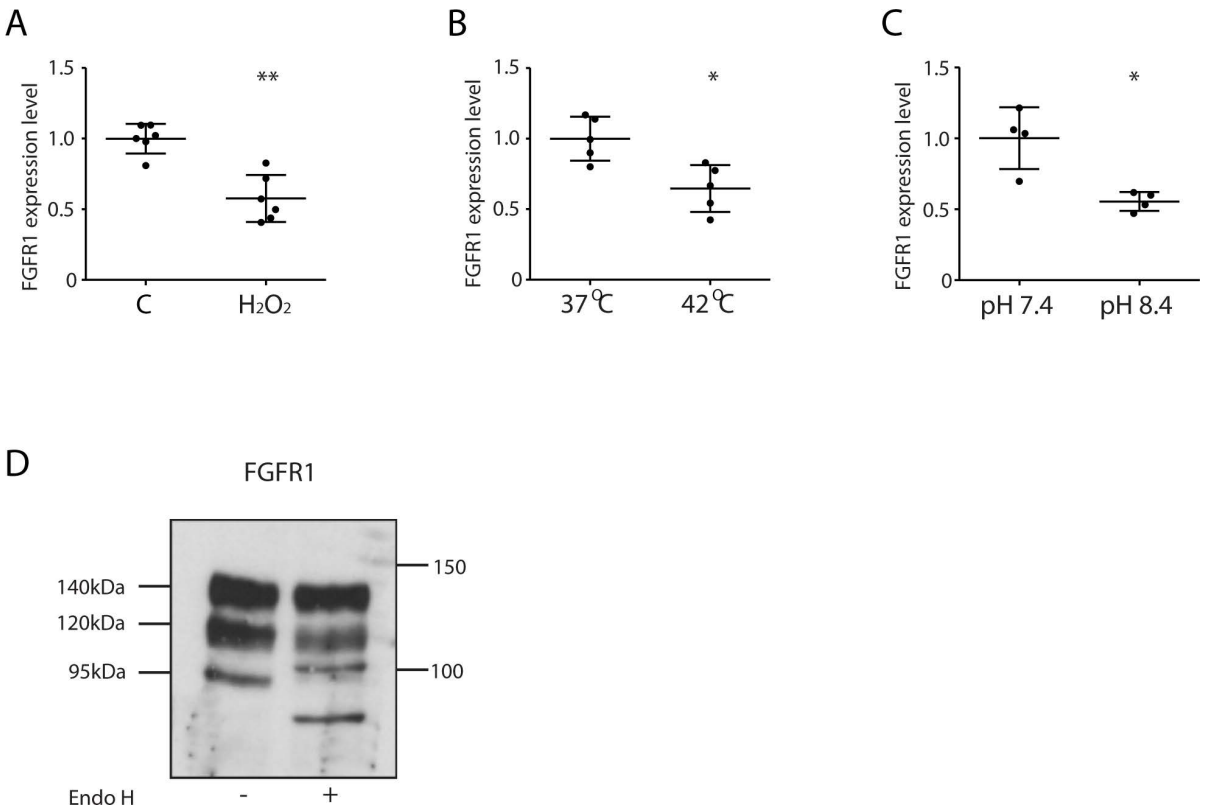

Figure S5. Quantification of FGFR1 Protein Levels in Embryos and Cells by Immunoblot. Related to Figure 5.

(A-C) Quantification graphs for FGFR1 in cells exposed for 2 hours to (A) 0.1 mM hydrogen peroxide, (B) heat shock at 420C, or (C) alkaline pH (culture under 0.1% CO2 atmosphere). (D) Immunoblot of endogenous FGFR1 in mouse muscle satellite C2C12 cells. Three bands are detected (140 kDa, 120 kDa and 95 kDa; left lane). Endoglycosidase H (Endo H; right lane) does not cleave the fully glycosylated 140 kDA polypeptide, but does cleave the partially glycosylated (120 kDa, 95 kDa) polypeptides. Molecular marker sizes are shown in kDa. Graph shows mean and standard deviation. * $p<0.05$, ** $p<0.01$.

Table S1. Short term Gestational Hypoxia Induces Heart Defects

				Type of heart defect observed								
Exposure stage	Embryos examined	Normal	Abnormal	VSD	muscular VSD	OA	DORV	TGA	ASD	PTA	SOTV	TVA
control	33	31	2	2	1	0	0	0	0	0	0	0
E7.5	27	27	0	0	0	0	0	0	0	0	0	0
E8.5	40	33	7	6	1	3	2	1	1	0	2	0
E9.5	48	27	21	18	1	7	10	3	3	1	1	1
E10.5	36	29	7	5	2	2	0	0	2	0	3	0

Note that a particular embryo may have more than one type of defect.

Pregnant mice were exposed to 5.5% oxygen for 8 hours on the indicated day of gestation. Mice were returned to normoxia, and embryos allowed to develop until E17.5, when heart morphology was analyzed. VSD: membranous ventricular septal defect; muscular VSD: muscular ventricular septal defect; OA: overriding aorta; DORV: double-outlet right ventricle; TGA: transposition of the great arteries; ASD: atrial septal defect; PTA: persistent truncus arteriosus; SOTV: straddling overriding tricuspid valve; TVA: tricuspid valve atresia

SUPPLEMENTAL MATERIALS AND METHODS

Optical projection tomography

For analysis of E10.5 OFTs, embryo torsos immunostained with MF 20 were dehydrated in methanol and cleared for at least 24 hours in 1:2 benzoic acid/benzyl benzoate (BABB). These were superglued directly to the mounting post of the OPT scanner. For whole E17.5 hearts, hearts were dissected from Bouin's fixed embryos stored in 70% ethanol, rehydrated to water, then dehydrated in methanol and cleared in BABB for at least 24 hours. Single hearts were placed in a cut-off and sealed glass Pasteur pipette, and attached to the mounting post. OPT scanning was performed using a custom microscope controlled by purpose-built software OPTimum (James Springfield, Institute for Molecular Biosciences, University of Queensland, Australia). 800-1,200 images in the FITC channel were collected per sample. These were reconstructed using nRecon (Bruker microCT, Belgium). Data were rendered in Amira 5.5.0 (FEI Visualization Services Group, USA). E17.5 heart morphology was analyzed directly in Amira. To quantitate OFT dimensions, reconstructions of OFTs were first rotated to the same orientation using Amira. 2D views were then exported in PNG format, and the OFT angle and length measured using ImageJ 1.49 (NIH, USA).

Immunohistochemistry

For immunohistochemistry, embryos were harvested at E9.5, fixed overnight in 4% paraformaldehyde at 4^{O}C, paraffin embedded and sectioned in the sagittal plane. To minimize inter-slide staining variation, tissue arrays were made by putting single sections from 12-20 different embryos on a single slide, and slides were processed using a Shandon Sequenza® Immunostaining Center (Thermo Scientific). Antigen retrieval for all antibodies except active/pro Caspase 3 was done using TE buffer (Moreau et al., 2014). For active/pro Caspase 3, slides were boiled in 10 mM Sodium Citrate, 0.05% Tween 20, pH 6.0 for 25 minutes. Slides were mounted in Mowiol® with DABCO (Allan, 1999). Images were captured on either a LSM 7 Duo or a LSM 710 upright confocal microscope (Carl Zeiss).uFor detecting FGFR1 or HIF1α in paraffin sections, biotinylated donkey anti-rabbit secondary and streptavidin Cy3 tertiary reagents were used. For detecting active/pro Caspase 3 and Hypoxyprobe™ in paraffin sections, ImmPRESS™ secondary reagent and 3-amino-9-ethylcarbazole (AEC for Caspase 3; Sigma Aldrich) or 3, 3'-diaminobenzidine (DAB for Hypoxyprobe™; Sigma Aldrich) was used.

Table S2. Antibodies used for immunodetection

Target	Name	Catalog number	Species and type	Supplier	Dilution for IHC	Dilution for IB
Primary antibodies						
active/pro Caspase 3		ab13847	rabbit polyclonal	Abcam	1:200	na
Myosin II heavy chain	MF 20		mouse monoclonal	Developmental Studies Hybridoma Bank	1:100	na
phospho-histone H3	(Ser 10)-R	sc-8656	rabbit polyclonal	Santa Cruz Biotechnology	1:200	na
phospho-p44/42 MAPK (Erk1/2) (Thr202/Tyr204)	D13.14.4E	4370	rabbit monoclonal	Cell Signaling Technology	1:200	1:1,000
p44/42 MAPK (Erk1/2)		9102	rabbit polyclonal	Cell Signaling Technology	na	1:1,000
FGFR1	D8E4	9740	rabbit monoclonal	Cell Signaling Technology	1:400	1:1,500
GM130		610822	mouse monoclonal	BD Transduction Laboratories	1:400	na
PDGFRß	958	sc-432	rabbit polyclonal	Santa Cruz Biotechnology	1:50	na
Hypoxyprobe ™ FITC	4.3.11.3		Mouse monoclonal	Hypoxyprobe, Inc.	1:400	na
HIF1α		NB100-449	rabbit polyclonal	Novus Biologicals	1:400	na
DDIT3	F-168	sc-575	rabbit polyclonal	Santa Cruz Biotechnology	1:50	1:500
phospho eIF2α (Ser51)	D9G8	3398	rabbit monoclonal	Cell Signaling Technology	na	1:1,000
ß-tubulin	E7		mouse monoclonal	Developmental Studies Hybridoma Bank	na	1:500
FLAG®	M2	F1804	mouse monoclonal	Sigma-Aldrich	na	1:1,000
Secondary Antibodies						
Donkey anti-		711-165-		Jackson	1:500	na

rabbit Cy™3		152		ImmunoResearch		
Donkey anti-goat AlexaFluor® 488		A-11055		Life Technologies	1:500	na
Donkey anti-mouse AlexaFluor ® 488		715-545-151		Jackson ImmunoResearch	1:500	na
Goat anti-mouse IRDye® 800CW		926-32210		LI-COR	na	1:10,000
Goat anti-rabbit AlexaFluor® 680		A-21109		Life Technologies	na	1:5,000
Donkey anti-rabbit biotinylated		711-065-152		Jackson ImmunoResearch	1:500	na
ImmPRESS™ (Peroxidase) Polymer anti-mouse Ig Reagent		MP-7402		Vector Laboratories	1:1	na
ImmPRESS™ (Peroxidase) Polymer anti-rabbit Ig Reagent		MP-7401		Vector Laboratories	1:1	na
Tertiary reagents						
Steptavidin Cy™3		GTX85902		GeneTex	1:1,000	na
Nuclear stain						
TO-PRO®-3 Iodide		T3605		Life Technologies	1:10,000	na

RNA *in situ* hybridization probes

cDNA probes used were as follows: *Spry1* (Addgene plasmid # 22091, Minowada et al., 1999)), *Spry2* (Addgene plasmid # 22097, Minowada et al., 1999), *Spry4* (Addgene plasmid # 22093, (Minowada et al., 1999), and *Fgf8* (Mahmood et al., 1995).

Cell culture and immunoblots

Mouse muscle satellite C2C12 cells (ATCC) were cultured in IMDM medium with glutamine (Life Technologies) and 10% fetal bovine serum (Life Technologies) on 40 mm Steriplan®

glass petri dishes (DURAN) in 5% CO_2. C2C12 cells were verified as free from mycoplasma contamination using the MycoAlert Detection Kit (Lonza). Hypoxic exposure of cells was done using a H35 Hypoxystation (Don Whitley Scientific). Culture medium was equilibrated in 0.1% O_2 overnight prior to use. Culture dishes were transferred to the workstation, rinsed once with hypoxia-equilibrated medium, and incubated in fresh hypoxia-equilibrated medium for the indicated times. For the study of UPR inhibitors, cells were incubated for 2 hours in the normoxic or hypoxia-equilibrated medium containing 20 μM IRE1 inhibitor 4μ8c (Sigma Aldrich) or 1 μM PERK inhibitor GSK2606414 (Selleck Chemicals) or equivalent volume of DMSO as a control. Whole cell protein extracts and immunoblots were performed by standard methods, with detection using either HRP-labeled secondary antibodies and SuperSignal West Pico chemiluminescent substrate (Thermo Fisher) or fluorescently-labeled secondary antibodies and the Li-Cor Odyssey Infrared Imaging System.

Quantification methods

Staining intensity of immunohistochemistry on paraffin sections was quantified using ImageJ 1.49 (NIH, USA). Briefly, LSM files generated by confocal microscopy were imported into ImageJ. The region of interest (ROI) was manually defined, and the image was threshholded to remove background. Identical threshholding values were used for all images of each experiment. The signal above threshold was quantified, and normalized to ROI area. For quantitation of FGFR1 proteins levels in the Golgi, stacks of confocal LSM images from sections co-stained with FGFR1 and GM130 were imported into ImageJ. The ROI was manually defined in the GM130 channel, and all signal outside this area was removed. The GM130 channel was threshholded to remove background, using identical values for all images, and the intensity of GM130 staining quantified. The area of GM130 staining in the ROI was used to make a selection mask, which was then applied to the FGFR1 channel. The FGFR1 channel was threshholded to remove background using identical values for all images, and the intensity of FGFR1 staining in the GM130-expresing domain of the ROI was quantified. For proliferation measurement, the percentage of phospho-histone H3 positive cells in each embryo was calculated as the ratio of combined total number of phospho-histone H3 positive cells against the combined total number To-Pro3+ nuclei from three independent sections from the same embryo. Staining intensity of RNA wholemount *in situ* hybridization images was also quantified using ImageJ. Stained embryos were photographed using a M125 dissection microscope with DFC450 camera (Leica microsystems GmbH, Germany), using

identical lighting and camera settings for all embryos stained for the same transcript. TIFF files were imported into ImageJ and changed to 8-bit grayscale. The ROI was manually defined, threshholded to remove background with identical settings for all images, and the integrated density in the ROI measured. Immunoblots analyzed by chemiluminescence were digitized using a FLA-5100 scanner (Fujifilm, Japan), and converted to TIFF format using ImageJ. Immunoblots analyzed by Odyssey Imager (LI-COR) were scanned at high resolution and saved as TIFF files. In both cases, bands were quantitated using Gelanalyzer (gelanalyzer.com).

Analysis of embryonic apoptosis

Two adjacent sagittal sections of each embryo (n=10 control and n=10 exposed) were stained for active/pro Caspase 3 and the other for TUNEL. These were taken from roughly the same sagittal plane from every embryo to ensure a similar area was surveyed across all embryos. One view field per section was counted for each of the SHF, OFT, ventricular myocardium, posterior part of the neural tube, otic vesicle and gut.

SUPPLEMENTARY REFERENCES

Mahmood, R., Bresnick, J., Hornbruch, A., Mahony, C., Morton, N., Colquhoun, K., Martin, P., Lumsden, A., Dickson, C., and Mason, I. (1995). A Role for Fgf-8 in the Initiation and Maintenance of Vertebrate Limb Bud Outgrowth. Curr Biol *5*, 797-806.

Minowada, G., Jarvis, L.A., Chi, C.L., Neubuser, A., Sun, X., Hacohen, N., Krasnow, M.A., and Martin, G.R. (1999). Vertebrate Sprouty Genes Are Induced by Fgf Signaling and Can Cause Chondrodysplasia When Overexpressed. Development *126*, 4465-4475.

Allan, V.J. (1999) *Protein Localization by Fluoresence Microscopy*, Oxford, United Kingdom: Oxford University Press.

Moreau, J. L., Artap, S. T., Shi, H., Chapman, G., Leone, G., Sparrow, D. B. and Dunwoodie, S. L. (2014) 'Cited2 is required in trophoblasts for correct placental capillary patterning', *Dev Biol* 392(1): 62-79.